Highly Accurate Potential Energy Surface, Dipole Moment Surface, Rovibrational Energy Levels, and Infrared Line List for $^{32}S^{16}O_2$ up to 8000 cm^{-1}

Xinchuan Huang (黄新川),[1a*] David W. Schwenke,[2b] and Timothy J. Lee[3c*]

[a] SETI Institute, 189 Bernardo Ave, Suite #100, Mountain View, CA 94043, USA
[b] MS T27B-1, NAS Facility, NASA Ames Research Center, Moffett Field, CA 94035, USA
[c] MS 245-1, Space Science and Astrobiology Division, NASA Ames Research Center, Moffett Field, CA 94035, USA

Submitted to: *J. Chem. Phys.*

[1] Corresponding Author: Xinchuan.Huang-1@nasa.gov

[2] Email: David.W.Schwenke@nasa.gov

[3] Corresponding Author: Timothy.J.Lee@nasa.gov

Abstract

A purely *ab initio* potential energy surface (PES) was refined with selected $^{32}S^{16}O_2$ HITRAN data. Compared to HITRAN, the root-mean-squares error (σ_{RMS}) error for all J=0-80 rovibrational energy levels computed on the refined PES (denoted Ames-1) is 0.013 cm^{-1}. Combined with a CCSD(T)/aug-cc-pV(Q+d)Z dipole moment surface (DMS), an infrared (IR) line list (denoted Ames-296K) has been computed at 296K and covers up to 8,000 cm^{-1}. Compared to the HITRAN and CDMS databases, the intensity agreement for most vibrational bands is better than 85-90%. Our predictions for $^{34}S^{16}O_2$ band origins, higher energy $^{32}S^{16}O_2$ band origins and missing $^{32}S^{16}O_2$ IR bands have been verified by most recent experiments and available HITRAN data. We conclude that the Ames-1 PES is able to predict $^{32/34}S^{16}O_2$ band origins below 5500 cm^{-1} with 0.01-0.03 cm^{-1} uncertainties, and the Ames-296K line list provides continuous, reliable and accurate IR simulations. The K_a-dependence of both line position and line intensity errors is discussed. The line list will greatly facilitate SO_2 IR spectral experimental analysis, as well as elimination of SO_2 lines in high-resolution astronomical observations.

I. Introduction

Life as we know it cannot exist without several key chemical elements, one of which is sulfur, and the most important sulfur-containing molecule in many space environments is sulfur dioxide, SO_2 [1,2,3,4,5,6,7,8,9,[10]]. Determination from experimental or theoretical investigations of fundamental atomic, molecular, and nuclear parameters is important for the analysis of NASA's space data obtained by the Spitzer Space Telescope (SST), the Stratospheric Observatory for Infrared Astronomy (SOFIA), and the Herschel Space Observatory (HSO), as well as other past and future NASA and ESA space science missions.

The Herschel Space Observatory (HSO) opened an exciting new window into the universe: continuous wavelength coverage from 60-670 μm with tremendous sensitivity without any atmospheric interference. This spectral range is the playground of molecules, and the potential for significant new discoveries in astrophysics and astrobiology is huge. While HSO has completed its mission, analysis of data from the mission continues – for example see Refs.[9,11,12] for recent studies that identify molecules based on HSO data.

Of the instruments on Herschel, HIFI covers the spectral range 480-1250 GHz (240-625 μm or 16-42 cm^{-1}) and 1410-1910 GHz (157-213 μm or 47-64 cm^{-1}), and can achieve very high resolution (circa 1 MHz). With the increasingly higher resolution of the latest missions and telescopes, positive identification of molecules will be possible as well as the determination of fine details of the environment in which the species exist. The challenge will be to separate out the features of interest from the multitude of interfering transitions. The problem is that while only a handful of lines are required for the definitive detection of a molecule, a complete characterization of the spectrum is required to subtract out the contribution of a molecule that contributes many, many transitions in order to reveal what lies beneath.

The report from the workshop on laboratory spectroscopy in support of Herschel, SOFIA and ALMA clearly lays out the problem [13]. "For observations of the dense regions in which star formation occurs, the youngest stars and the protoplanetary disk material surrounding them possess spectra containing a few molecular species with extremely numerous, relatively strong transitions throughout the submillimeter. These species are likely to present a serious challenge, in as much as their emission will occupy a substantial part of the spectral range available, thus impeding the study of other important species. Thus, the discovery of new species of astrophysical and astrobiological interest will be severely hampered unless the spectral lines from these 'weeds' can be removed from the data." This report goes on to identify the four most prominent (Class 1) weeds, and five somewhat less prominent (Class 2) weeds. Sulfur dioxide is a Class 2 weed. The report further states that the spectra of the weeds and all their isotopologues are required, that quantum number assignments must be made for all transitions, and that the weeds are expected to be associated with temperatures primarily in the 100-300 K range.

In this work, we are directly responding to the need of observers by combining the state-of-the-art quantum chemical method with reliable high-resolution experimental data. While theoretical calculations have been carried out for many years, recent advancements in algorithms, computer hardware, and theoretical formulations have made the accurate prediction of molecular spectra closer than ever. Recently we reported that the “best theory plus high-resolution experiment” strategy has been successfully extended from H_2O [14,15], NH_3 [16,17,18,19,20] to CO_2 [21,22]. Near 7000 experimentally measured CO_2 energy levels up to J=117 and 14,320 cm^{-1} were reproduced with σ_{RMS} = 0.0156 cm^{-1}. The $^{12}C^{16}O_2$ Ames-296K line list predictions near 9000 cm^{-1} has been verified by recent experiments [23] as more reliable than old HITRAN model.[22] Relative to CO_2, much less high-resolution experimental infrared (IR) rovibrational data is available for SO_2. HITRAN2008 [24] and HITRAN2012 [25] are essentially the same for SO_2 which only have 13 vibrational states and 14 associated IR bands in the 0 - 4200 cm^{-1}

spectral range. The purpose of the present study is to provide a high quality line list plus IR intensities for SO_2 that is suitable for analyzing astronomically observed spectral data from Spitzer, Herschel, and SOFIA, and for modeling higher energy and high-temperature spectra. Note that this SO_2 study is not limited to the far-IR range of HIFI or ALMA, but rather we will cover the range 0-7000 cm^{-1} in this initial study with J=0-80 for most bands. The demand for quantum number assignments and data for all isotopologues is tailor made for the type of approach that we have previously used for the H_2O, NH_3, and CO_2 molecules.

The primary purpose for spectral data of the weeds is to remove their influence from measured spectra to reveal the "flowers", but once given our results, new possibilities exist. For example, one could use the measured spectra of SO_2, which would normally be thrown away, and use it to obtain more detail about isotopic abundances. It is well known that isotopic abundances reflect the origin of species, and the weeds with their bright spectra might make a particularly sensitive probe to some very interesting processes.

While our primary purpose has been to generate SO_2 line lists that will be useful in analyzing high-resolution astronomical spectra, we note that SO_2 is of great interest in planetary atmospheres as well, especially Venus and exoplanet atmospheres. In fact, SO_2 is the second major component of the Venus atmosphere and the SOIR instrument on the Venus Express mission measures high-resolution spectra in the 2400-4400 cm^{-1} region, which includes a CO_2 window. Both the ExoMol database [26] and Exoplanet Characterization Observatory (EChO, an ESA mission candidate) [27] consider generation of a SO_2 line list an important need for the community. Additionally, monitoring the SO_2 emission generated by power stations on Earth is also a critical focus for environment protection. Unfortunately, HITRAN has very little coverage for SO_2, and thus it is expected that our line lists will also be useful in analyzing Venus Express data from the SOIR instrument, the modeling of exoplanet atmospheres, and potentially for use in the monitoring of power stations on Earth.

In this paper, we present a refined spectroscopically accurate potential energy surface (PES) for $^{12}S^{16}O_2$, denoted Ames-1, as well as an Ames-296K IR line list computed with an *ab initio* dipole moment surface (DMS) without any refinement. Section II describes the theoretical approach adopted in the present work, which is similar to that used previously for NH_3 and CO_2 [17,21], so only an abbreviated description is given in Section II. Several technical details are described in section III, followed by results and discussion in section IV. A summary and future work is presented in the final section.

It should be noted that this study serves as a basis for future SO_2 studies, e.g. a far-IR simulation with even higher accuracy for both line positions and line intensities, as well as studies that cover a larger spectral range and include higher J values, which will be needed to model high-temperature spectra of SO_2.

II. Theory and Algorithm

At NASA Ames, the “Best Theory + High-resolution Experimental Data” strategy has yielded σ_{rms}< 0.05 cm^{-1} for H_2O line positions,[14] and better than 95% accuracy for H_2O IR line intensities.[28] The water line lists generated in Ref.14 and Ref.28 greatly contributed to the growth and purification of water spectral databases.[15,29] For $^{14}NH_3$, σ_{rms} = 0.02 cm^{-1} for 6000 transitions arising from ground state levels, and σ_{rms}=0.04 cm^{-1} for 1790 “hot-band” transitions arising from ν_2 levels.[17,18] For $^{12}C^{16}O_2$, σ_{rms} = 0.0156 cm^{-1} for 6873 purely expt-based rovibrational levels and better than 80% intensity agreement for more than 80% of 231 experimentally measured bands.[21]

However, the key point goes beyond simply reproducing the included experimental data. Much more importantly, our focus has been to provide reliable analysis and predictions for unknown bands and isotopologues, as well as identifying incorrect assignments, with *the same accuracy as for directly observed experimental data*. This degree of unprecedented accuracy (i.e. 0.01 – 0.02 cm^{-1}, or at least better than 0.05 cm^{-1}) is critically important as it is required

to aid in the reliable analysis of high-resolution observational data (for example, see Ref.19 where new assignments for NH_3 were aided by our earlier work). More interestingly, a recent CO_2 experiment has confirmed the validity of our IR line list at ~9000 cm^{-1} where HITRAN2008 IR intensities exhibited errors of two orders of magnitude.[23] Currently, purely *ab initio* theory is not capable of providing $\sigma_{rms} < 0.1$ cm^{-1} accuracy for the rovibrational spectra of polyatomics, except for the two-electron system H_3^+. Therefore, high-quality *ab initio* PES's need to be refined with high-resolution experimental data. Additionally, the DMS needs to be critically examined in order to achieve excellent agreement with measured band intensities. Specifically, the shape of the DMS will be different to that of the PES, and thus the grid one uses will necessarily be different.

Many technical aspects are involved in the procedure. One critical part is to solve the full-dimensional quantum rovibrational Hamiltonian equations (within the Born-Oppenheimer approximation) accurately, and efficiently. Both rovibrational energies and wavefunctions have to be well converged before, during, and after the refinement procedure. Approximations in solving the nuclear Schrödinger equation can easily lead to unpredictable noise in the results, which ultimately degrades the reliability and precision of the line positions predicted. The VTET program used in this work solves the nuclear Schrödinger equation with an efficiently contracted basis, and converges the rovibrational energies well. It then saves the wavefunctions for use in the refinement step. Interested readers are referred to Ref.[30] for more details. It should be further noted that even higher convergence criteria should be adopted for the wavefunctions to be used in intensity computations, because our goal is to provide reliable predictions for IR spectra beyond current experimental limits.

III. Technical Details

III.1 *Ab initio* calculations and choice of the starting purely *ab initio* PES

We started from singles and doubles coupled-cluster with perturbative triples, CCSD(T) [31] calculations plus various small corrections. In total, 489 geometries were selected after our initial PES studies exploring extremely high energy regions and the quality of the coverage of the PES, including one-dimensional potential cuts. On every single point, CCSD(T) calculations were carried out with the following correlation consistent basis sets: cc-pV(*X*+d)Z,[32,33] aug-cc-pV*X*Z,[34 , 35] *X*=T,Q,5; aug-cc-pwCV*X*Z,[36] *X*=T,Q; cc-pVQZ-DK[33] for the scalar relativistic correction;[37] and the Martin-Taylor basis for core-correlation effects.[38] In the end we have 26 global *ab initio* PESs for SO_2, plus 26 more PES if the scalar relativistic correction is included. In order to find the best starting PES to use in the empirical refinement, vibrational variational configuration interaction (CI) results were compared to a set of 125 low-resolution vibrational band origins up to 6900 cm^{-1}. The band origin set is summarized in Ref.[39], but it is not really a high/medium resolution estimate. Instead, it is essentially tracked back to the Dunham expansion formula and anharmonic constants derived from Shelton, Nielsen and Fletcher's experimental work in 1953 [40], which were fitted from 17 observed band centers. However, the current upper wavenumber limit of $^{32}S^{16}O_2$ high-resolution IR data is below 4300 cm^{-1}, and the reliability of this reference set is estimated to be a few cm^{-1}. We conclude it is acceptable for the selection of our purely *ab initio* PES.

As described above, J=0 vibrational calculations were carried out on all PESs and the computed *J*=0 states were compared to the 125 vibrational terms from 0 to 6900 cm^{-1}. In the end, the CCSD(T)/cc-pVQZ-DK PES fit was selected since it had the smallest average deviation: 5.34 cm^{-1} and 0.11% for all 125 states. Other choices (based on the CCSD(T) method) include: aug-cc-pV(Q+d)Z (6.30 cm^{-1}, 0.13%), aug-cc-pwCVQZ (5.40 cm^{-1}, 0.11%), cc-pV(Q+d)Z+rel (5.90 cm^{-1}, 0.13%), aug-cc-pV(5+d)Z+rel (6.89 cm-1, 0.14%), or aug-cc-pwCVQZ (with core)+rel (7.14 cm^{-1}, 0.14%). All other PESs had relative errors >0.20%. Similar to $^{12}C^{16}O_2$,[21] $^{32}S^{16}O_2$ becomes our 2nd

molecule where a QZ level PES has exhibited the best error cancellation, while a PES that includes extrapolation to the one-particle basis set limit [41] yields larger errors. Using the CCSD(T)/cc-pVQZ-DK PES fit, we estimate that the main effects being cancelled out include core-correlation and one-particle basis set deficiencies common to second-row atoms,[42] while some smaller effects include extrapolation to the complete basis set limit, inclusion of diffuse functions in the basis set, and higher-order correlation effects.

III.2 Least-squares fit and PES representation

To obtain a highly-accurate, realistic and *global* PES, we divide the PES into short range terms and long range terms, i.e. V_{Short} and V_{Long}.

$$V = V_{\text{Short}} + V_{\text{Long}}.$$

We follow previous work on H_2O[14], NH_3[16,17] and CO_2 [21] regarding the choice of V_{long} and V_{short} formulas, as well as the weight function used in the least-squares fit. 400 of 489 final points below 30,000 cm^{-1} are more heavily weighted:

$$s = [\tanh(-0.00045 - 3\cdot(E - 30000)) + 1.00200200]/2.00200200$$
$$weight = s / \max(E, 30000)$$

where E is the potential in cm^{-1} related to the C_{2v} minimum.

The long-range part, V_{Long}, is based on a simple Morse-potential model plus a simple bending model:

$$V_{Long} = \sum_{i=1}^{2} D_{e1}(1 - e^{-\beta\cdot\Delta r_i})^2 + \sum_{i=1}^{2} D_{e2}(1 - e^{-\beta\cdot\Delta r_i})^4 + e^{-0.2\cdot(\Delta r_1^2 + \Delta r_2^2)}\cdot(A_{e1}\Delta a_1^{\,2} + A_{e2}\Delta a_1^{\,4})$$

where

$$D_{e1} = 233{,}156\ cm^{-1},\ D_{e2} = 5{,}250\ cm^{-1},\ A_{e1} = 56{,}000\ cm^{-1},\ A_{e2} = 50{,}000\ cm^{-1}$$
$$\beta = 1.152733\ Å^{-1},\quad \Delta r_i = r_i - r_{ref},\quad r_{ref} = 1.43108\ Å,\ \Delta a_1 = \cos\alpha_{\angle OSO} - \cos(119.3209°)$$

r and α represent the S-O bond length in Å and the ∠OSO, respectively. The choice of D_{e1} and D_{e2} are obviously much higher than the S=O bond dissociation energy, mainly in order to ensure that the final PES is globally positive in the dissociation region where the short range terms have already been damped out.

The V_{Short} terms are damped out as any S-O bond dissociates or the ∠OSO is strongly bent. The criterion used for selecting these damping parameters is the final σ_{rms} error for the most important energy region, that is 0 – 30,000 cm^{-1}. Mathematically, V_{Short} is given by:

$$V_{Short} = f_{damp}\sum_{n=1}^{219} C_{ijk}^{n} P[(\Delta r_1)^i(\Delta r_2)^j](\Delta\alpha_1)^k$$
$$f_{damp} = e^{-damp1\sum_{i=1}^{2}(\Delta r_i)^2 - damp2\sum_{i=1}^{2}(\Delta r_i)^4 - damp3\cdot(\Delta\alpha_1)^2 - damp4\cdot(\Delta\alpha_1)^4}$$

where

$$damp1 = 1.5,\ damp2 = 3.0,\ damp3 = 0.1,\ damp4 = 0.3,\ r \text{ in Å and } \alpha \text{ in radians}$$
$$\beta = 1.0\ Å^{-1},\ \Delta r_i = r_i - 1.43108\ Å,\ \Delta\alpha_1 = \cos\alpha_{\angle OSO} - \cos(119.3209°)$$

and P is the permutation operator that ensures that $P[(\Delta r_1)^i(\Delta r_2)^j]$ is totally invariant with respect to the interchange of the two O atoms. We note that the PES extends beyond 20,000 cm^{-1}, because it is necessary in order to properly describe the rovibrational energy levels up to 10,000 cm^{-1}. That is, the value of vibrational energy levels near 10,000 cm^{-1} are impacted to a small extent by the shape of the PES at higher energies, hence the need for the PES to extend to higher energies.

The final PES includes 219 coefficients. For the indices i, j, and k, we have $0 \le i,k \le 8$, $j \le i$, and $i+j+k \le 12$. An additional set of 31 boundary points were included in the least-squares fit (with a 1/100 fitting weight) to ensure the final fitted PES is globally positive. When fitting to the original *ab initio* CCSD(T)/cc-pVQZ-DK energies, the average fitting deviation (absolute value) for the 393 *ab initio* energy points below 30,000 cm^{-1} is 0.21 cm^{-1}, while the σ_{rms} error is 0.31 cm^{-1}.

III.3 The Purely ab intio DMS

On the refined PES, 3928 geometries were randomly generated in the 0 - 60,000 cm^{-1} range. The number of points selected in each 1000 cm^{-1} interval monotonically decreases from 126 in 1000 - 2000 cm^{-1} to 18 in 59,000 - 60,000 cm^{-1}. From 0 to 30,000 cm^{-1}, there are 2881 points. CCSD(T)/aug-cc-pV(Q+d)Z finite-field dipole calculations were run on these points and thus there are 3638 dipoles to be used in a least-squares fit. It is well known that electrical properties, such as the dipole moment or polarizabilities, require a better description of the diffuse part of the wavefunction, which is why the aug-cc-pV(Q+d)Z basis set was used. The dipole moments were computed as the energy derivatives with respect to an external electric field.

Similar to our CO_2 work [21], the DMS was fit according to a pseudo-point-charge-on-nuclei model in order to maintain the permutation symmetry of the two O atoms. The same permutation invariant strategy was adopted previously for the $H_5O_2^+$ dipole moment surface fit.[43] The S atom is fixed at the origin of the Cartesian system and the point charge on an O atom is expanded in bond length changes Δr_1, Δr_2, and bond angle displacements $\Delta a_1 = \cos\alpha_{\angle OSO} - \cos(119.32°)$. Then the sums of the charge-position vector product on the two O atoms are fitted to *ab initio* dipole values.

$$\vec{\mu} = q_{O1} \cdot \vec{r}_1 + q_{O2} \cdot \vec{r}_2 + q_S \cdot \vec{r}_S = q_{O1} \cdot \vec{r}_1 + q_{O2} \cdot \vec{r}_2$$

$$q_{O1} = \sum_{n=1}^{969} C_{ijk}^n \Delta r_1^{\,i} \Delta r_2^{\,j} (1 + \cos\alpha_{\angle OSO})^k$$

$$q_{O2} = \sum_{n=1}^{969} C_{ijk}^n \Delta r_2^{\,i} \Delta r_1^{\,j} (1 + \cos\alpha_{\angle OSO})^k$$

where $\Delta r = r - 1.43108$ Å, $0 \le i+j+k \le 16$. In total there are 969 C_{ijk}^n coefficients for the $q_{O1/O2}$ expansion formula. The fitted dipoles are invariant to the permutation of the two O atoms. The weighting scheme from the PES fit was applied in order to focus on the region below 30,000 cm^{-1}, for which the average fitting error and average relative error are as small as 1.8×10^{-5} a.u. and 0.010 %, respectively. The corresponding root-mean-square (RMS) errors σ_{rms} are 3.0×10^{-5} a.u. and 0.082 %.

This purely *ab initio* dipole surface has been utilized in rovibrational intensity calculations to generate an initial IR line list at 296K, denoted Ames-296K. By comparing with available experimental spectra and databases, we can find potential defects of the DMS for future improvements. Given that this is a starting DMS, it is fairly accurate, while some improvements may be required, especially for future high energy and high temperature simulations. See more details in the Results and Discussion section.

III.4 HITRAN2008/2012 Bands, Intensities, and Energy levels

The HITRAN-2008 and HITRAN-2012 databases [24,25] include transition frequencies and intensities of 14 bands at 296K. Pure rotational bands ν_2=0 and ν_2=1 were taken from the CDMS[44] database, plus 7 bands arising from the ground state (GS) and 5 "hot" bands arising from ν_2=1. In the 13 related vibrational states, only the GS and ν_2=1 pure rotational transitions have the highest J = 99. From J=0 to J=99, there are more than 13,000 rovibrational energy levels for $^{32}S^{16}O_2$, but not all of them are appropriate for our analysis. We have to remember that only a small

amount of data in CDMS and HITRAN were experimentally measured, while the remaining data were derived from experimental models. In our previous $^{12}C^{16}O_2$ Ames-1 PES study, we have shown that some model-based HITRAN data contain errors large enough to degrade significantly the empirical refinement.[21]

First we should note that the two purely rotational bands in HITRAN were completely taken from the CDMS database. Here, we first use the CDMS purely rotational energy levels to replace the lower state energies of all other HITRAN transitions. Then the HITRAN2008 database for $^{32}S^{16}O_2$ was transformed and filtered by a multi-determination width requirement (Δ(E_max – E_min) <0.01 cm^{-1}) to get a "reliable" set of rovibrational energy levels. In addition, the ierr parameter in HITRAN for line position uncertainty is adopted for further screening. Only those levels derived from ierr≥4 transitions are kept. This means the line position uncertainties are smaller than 1×10^{-3} cm^{-1}, which is good enough to compare with most rovibrational energy levels and transitions reported in this work.

In the present work, our calculations and analysis go up to J = 80. This is because it is only the first step for the high-temperature high-energy SO_2 IR line list project. J=80 should be good enough for room temperature IR line list simulations at 296K, as well as high enough to find potential defects in either the refinement or the line list. For *J*=0-80, there are 12,441 comparable HITRAN levels.

The high-resolution data we used in the SO_2 PES refinement were taken from HITRAN, at several discrete *J* values. In order to check the accuracy of the refined PES and line list, our predictions (including both interpolations and extrapolations) are compared to additional experimental data beyond HITRAN. After 2008, the Ulenikov group have published five high-resolution experimental papers covering 10 vibrational states: $3\nu_1$,[45] $3\nu_1+\nu_3$ and $\nu_1+3\nu_3$,[46] $2\nu_1+\nu_2+\nu_3$ and $\nu_2+3\nu_3$,[47] $3\nu_2$ and $\nu_1+2\nu_2$,[48] $\nu_1+3\nu_2$, $2\nu_1+\nu_2$, and $\nu_2+2\nu_3$.[49]. Different from HITRAN, only transmittance were reported and no absolute line intensities are available. Both published band origins and spectra have been compared side-by-side with our predictions and are reported in a later section.

III.5 Variational rovibrational and IR intensity calculations by VTET

Rovibrational energy levels, wavefunctions, and transition intensities were computed using the procedures described in Ref.[14]. We used hyperspherical Radau coordinates, with the S atom as the central atom, and we used the *llk* coupling scheme with maximum bending quantum number of 300. The angular matrix elements of the PES were determined analytically after making a 181 term Legendre expansion of the PES. This expansion was carried out numerically by Gaussian quadrature, with an average deviation between the re-expansion and original values being less than 10^{-12} a.u.

We optimized contracted basis functions for each *JPS* block. The cut off for solving the one-dimensional stretching Schrödinger equations were 0.187 Hartree, i.e. 41042 cm^{-1} (1 Hartree = 219,474.6 cm^{-1}) with error criterion 10^{-6} for determining the number of optimized quadrature points.[50] For each *K*, we kept all bending functions with energies below 0.15 Hartree (32921 cm^{-1}), and then we coupled these contracted functions, and kept all with energies below 0.12 Hartree (26337 cm^{-1}). The rotation-bending functions were made symmetry eigenfunctions as described previously.[14] The determination of the contracted stretching and bending functions was carried out iteratively until a self consistent value for the lowest energy for that particular *JPS* block. The excited functions were virtual levels of the ground state, i.e. all the other eigenfunctions of the Hamiltonian for the lowest energy (ground) state.

Finally we coupled the bending and stretching functions, including all functions whose sum of energies was no greater than 0.187 Hartree (41042 cm^{-1}), and extracted all roots with energies up to 0.06 Hartree (13168 cm^{-1}). Full permutation-inversion symmetry was exploited in this final diagonalization step.

In the intensity calculation, we used 24 point optimized quadrature for the stretches, and carried out the angular integrals analytically after making a 60 term associated Legendre expansion of the DMS. The expansion coefficients were determined numerically using a 72 point Gauss-Legendre quadrature.

III.7 Refinement

Similar to previous work,[17,21] we allow 21 coefficients (up to the quartic level) of the ***short-range*** potential expansion to vary. Initially, variations were limited to within a ±20% range, the limit we set in our NH_3/CO_2 refinements. However, this did not work out very well. The limitations were finally removed and all 21 coefficients were allowed to vary freely. This led us to conclude that the Ames-0 PES of $^{32}S^{16}O_2$ is more difficult to refine.

In those earliest trials, one refinement was carried out using J=0/4/10/20/70 Hamiltonian matrices and related "reliable" HITRAN energy levels. Ten Hamiltonian matrices and 30129 eigenvalues were involved. The total weighted σ_{RMS} error was reduced from 3.17 cm^{-1} to 0.010 cm^{-1}. Compared to the Ames-0 PES, nine coefficients were found changed by more than 20%: 521% for $\Delta_{Ra}{}^3\Delta_{Rb}$, -279% for $\Delta_{Ra}\Delta_\theta{}^3$, -287% for $\Delta_{Ra}{}^2\Delta_\theta{}^2$, 177% for $\Delta_{Ra}\Delta_{Rb}$, 121% for Δ_θ, 120% for $\Delta_\theta{}^2$, 61% for Δ_R, 42% for $\Delta_{Ra}{}^2\Delta_{Rb}\Delta_\theta$, and 41% for $\Delta_{Ra}{}^3\Delta_\theta$. Two coefficients for $\Delta_{Ra}\Delta_\theta{}^3$ and $\Delta_{Ra}{}^2\Delta_\theta{}^2$ had their signs changed. Note these relative changes are on short-range terms and they can be large. Usually they should be molecule specific and depend on the initial PES.

Because we were satisfied with this refinement, we computed energies of the fitted grid points on this primitive refinement, supplied these to the least-square fitting program together with the 31 pre-determined boundary points. The newly fitted PES was used to re-run the J=0/4/20/50/70 calculations. However, discrepancies of ~0.10 cm-1 were found between some refined energies (based on diagonzalized truncated Hamiltonian matrices) and the new variationally computed CI energies (based on the true exact quantum Hamiltonian within the Born-Oppenheimer approximation frame). We had used 1.4398 Å as the reference bond length for $R_{S\text{-}O}$ in the initial fitting, which is 0.6% longer than the final value 1.4310 Å. This 0.0087 Å difference is too large, and could probably account for the discrepancies we found here. In order to achieve better consistency, we carried out a 2nd-round of refinement using the new Hamiltonian matrices computed on the primitive refinement. Note that we run the re-fit with its exact minimum.

In this 2nd refinement based on the re-fit, 5/43/183/158/57 $^{32}S^{16}O_2$ levels were incorporated with 2.5/1.0/1.5/2.0/3.0 weights for J=0/4/20/50/70, respectively. Ten truncated Hamiltonian matrices (and 38467 eigenvalues) are computed at J=0/4/20/50/70. Accordingly, 80/73/49/47/43/30/22/74/28 levels were taken from GS/ν_3/$2\nu_3$/ν_2/$\nu_2+\nu_3$/$2\nu_2$/ν_1/$\nu_1+\nu_2$ states, respectively. An additional 19 high-resolution band origins were taken from Ref.45, including 5 repeated values for $2\nu_3$, ν_2, $2\nu_2$, ν_1 and $\nu_1+\nu_2$. In total, 465 reference values were used. Note that lower weights (0.01) were applied on 4/4/2 levels for J=20/50/70, though this does not mean the 10 reference values were wrong or unreliable. The apparent discrepancies were caused by a twisted order of roots. When the root order is corrected in the final refinement, the corresponding energies agree with HITRAN values to -0.01 - +0.02 cm^{-1}.

In the end, the weighted σ_{RMS} error was reduced from 0.13 cm^{-1} to 0.024 cm^{-1}, and the unweighted σ_{RMS} was reduced from 0.070 cm^{-1} to 0.010 cm^{-1}. It should be noted that the whole short-range expansion coefficients have changed during the re-fit, including higher order terms, so we do not compare to original *ab initio* values. Because the new base PES was fitted to its own minimum, both Δr_i and Δa_1 gradient coefficients are less than 2E-9 while their refined values are 1-2E-5, which are still relatively small. The largest changes are -218% for $\Delta_{Ra}\Delta_\theta{}^3$, -52% for $\Delta_{Ra}{}^2\Delta_\theta{}^2$, 123% for $\Delta_{Ra}{}^2\Delta_{Rb}\Delta_\theta$, -2743% for $\Delta_{Ra}{}^3\Delta_{Rb}$. Such large relative changes mainly result from their small magnitudes, e.g. -0.0192 ($\Delta_{Ra}\Delta_\theta{}^3$), +0.0121($\Delta_{Ra}{}^2\Delta_\theta{}^2$) and -0.53($\Delta_{Ra}{}^2\Delta_{Rb}\Delta_\theta$). The coefficient for $\Delta_{Ra}{}^3\Delta_{Rb}$ varies from -0.0041 (Ames-0) → -0.025 (first refined) → -0.0017 (refitted) → +0.046 (finally refined). All tests and calculations

up to now have not found any unreliability or mistakes that could be associated with these changes of the short-range PES terms.

IV. Results and Discussion

IV.1 Properties of Ames-1: Band origins

As mentioned above, 8 $^{32}S^{16}O_2$ vibrational states were included in the refinement. The refined Ames-1 PES predicts band origin G_0 term values with ~0.02 cm^{-1} uncertainty, for both interpolated bands and extrapolated bands beyond 4200 cm^{-1}, the HITRAN limit. See Fig.1, which includes everything experimental we have found that is high-resolution. It clearly shows that the accuracy achieved for $^{34}S^{16}O_2$ is essentially the same as that for $^{32}S^{16}O_2$. Similar accuracy for isotopic substitution was found for CO_2 where the $^{13}C^{16}O_2$ G_0 terms basically have the same accuracy as those of $^{12}C^{16}O_2$.

Full lists of Ames-1 J=0 vibrational band origins are given in Table 1 for both $^{32}S^{16}O_2$ and $^{34}S^{16}O_2$. High-resolution experimental data or experimental-model based values were taken mainly from Refs.[45,46,47,48,49,51,52] Note the G_0 term errors for certain bands that are included only for modeling purposes (i.e. not actually measured) can be as large as 0.1 – 1.0 cm^{-1}, e.g. $2\nu_1+2\nu_2$, $4\nu_2+\nu_3$, $\nu_1+4\nu_2$. Low-resolution "experimental" values (italic in parentheses in Table 1) were taken from Ref.[39] and were computed from Dunham expansion formula parameters taken from Ref.[40].

The largest deviations for $^{34}S^{16}O_2$ in Table 1 are the Δ(Ames-1 – Expt) = 0.0222 cm^{-1} for $\nu_1+\nu_3$ and 0.0487 cm^{-1} for $2\nu_1+\nu_3$. The corresponding $^{32}S^{16}O_2$ errors are 0.0206 cm^{-1} and 0.0255 cm^{-1}. For these relatively low-lying vibrational states, the relatively bigger discrepancy on $2\nu_1+\nu3$ between ^{32}S and ^{34}S isotopologues is suspicious. This assertion is based on our experience with CO_2, NH_3 and the other SO_2 band origins. If the experimentally modeled G_0 for $2\nu_1+\nu_3$ band (3598.7739 cm^{-1}) is verified by future experiments, we may need to investigate further the source of such isotopologue dependent discrepancies for the Ames-1 PES.

[Fig.1 Accuracy of Ames-1 PES: $^{32}S^{16}O_2$ and $^{34}S^{16}O_2$ band origins.]

[Table 1. $^{32/34}S^{16}O_2$ band origins up to 5165 cm^{-1}, computed on Ames-1 PES and compared with available experimental data. Note: new $^{32}S^{16}O_2$ band origins in Refs.45-49 and $^{34}S^{16}O_2$ band origins in Refs.51-52 were not included in the Ames-1 empirical refinement.]

The $\nu_1+3\nu_2$ band in $^{32}S^{16}O_2$ is unique because its K_a=11 levels and transitions are in strong resonance with the corresponding $2\nu_3$ K_a=11 values. No other K_a levels have ever been assigned for this band, which means its "experimental" band origin was actually derived from modeling, not directly observed. Extrapolation results from K_a=11 to J/K_a=0 largely depend on the specific Hamiltonian formula and spectral lines included. This may explain why the $\nu_1+3\nu_2$ band origins derived from two high-resolution experimental models differ by nearly 0.10 cm^{-1}. It easily explains the relatively larger uncertainty associated with this transition. Therefore, it is not really a surprise that Δ(Ames-1 – Expt) for $\nu_1+3\nu_2$ was the largest error for $^{32}S^{16}O_2$ in Table 1, i.e. 0.0511 cm^{-1}. The reference value adopted in our Ames-1 PES refinement (in 2011), 2693.6348 cm^{-1}, was taken from Ref.45, which in 2012 was updated to 2693.7279 cm^{-1}.[47] If we re-run the empirical refinement with 2693.7279 cm^{-1} as the corrected reference, the new $\nu_1+3\nu_2$ band origin on refined surface comes out at 2693.71 cm^{-1}, i.e. now the Δ is reduced to less than 0.02 cm^{-1}. These results strongly suggest the 2012 value (2693.7279 cm^{-1}) is probably more reliable than the previous one. On the other hand, although the refined Ames-1 PES was slightly perturbed by the misleading reference value, its self-correcting algorithm still yields a $\nu_1+3\nu_2$ band origin toward the right direction. This is a further evidence of the

robustness of our refinement procedure. Note that changing that specific reference value used in the refinement stage does not have any observable effects on the other HITRAN states because no other $\nu_1+3\nu_2$ $J/K_a>0$ levels were included in the fit and no other bands in HITRAN have higher quanta for both ν_1 and ν_2.

J=0 levels in Table 1 are cut off at 5165 cm^{-1}, which is the highest experimentally related energy. We fill in all missing band origins and assignments for both $^{32}S^{16}O_2$ and $^{34}S^{16}O_2$ so future experimental analyses can benefit from our reliable predictions. Average uncertainties for the predictions should be ~0.02 cm^{-1} or less. Due to the high density of states, a full list of both $^{32}S^{16}O_2$ and $^{34}S^{16}O_2$ J=0 states from the zero-point energy to 7000 cm^{-1} is provided in the supplementary EPAPS material.[53] We estimate the accuracy of those values will slowly degrade from ~0.02 cm^{-1} to 0.10-0.50 cm^{-1} at 7000 cm^{-1}, but only high-resolution experiments with definite low K_a lines can verify our predictions.

It should be emphasized that we deem the collaboration with experimentalists extremely important for such high resolution IR line list project, because close collaborations involving theoretical computations and experimental analyses will greatly facilitate and speed up construction of reliable IR line lists. For example, if 3-5 new band origins are experimentally determined near 7000 cm^{-1} and become available, performing a new refinement including these data will immediately guarantee that all the missing band origins between 5165 cm^{-1} - 7000 cm^{-1} may be predicted with better accuracy than we currently have.

IV.2 Properties of the Ames-1 PES: Geometry, dipole moment, and rotational constants.

Experimental dipole moment values and formula were given by Patel, Margolese and Dykea in 1979,[54] with a reported small uncertainty of 2-4×10^{-5} D. They have been widely accepted in spectral analysis and models, e.g. in CDMS. At the Ames-1 PES minimum, our fitted CCSD(T)/aug-cc-pV(Q+d)Z dipole is 1.629402 D, which is 0.16% larger than the experimental dipole 1.62673 D. Agreement for the equilibrium structure is excellent, 1.431086 Å / 119.319° (Ames-1) vs. experimental value 1.43076(13) Å / 119.33(1)° reported by Patel and co-workers in 1979.[55] Both the minimum structure and dipole we report here are in better agreement with experiment than the "best estimated" values predicted by Martin et al.[42].

For the vibrationally averaged structure and dipole, we are still within 1% errors. For the GS, ν_1, ν_2, and ν_3 levels (GS = ground state, i.e., the zero-point level), the experimental dipole values in Ref.[54] are 1.63305 D, 1.63322 D, 1.62614 D, and 1.65246 D, respectively. We did not compute these vibrationally averaged dipoles through a variational CI approach. Instead, we transformed the Ames-1 PES into a quartic force field (QFF; expanded around its exact minimum by 0.005 Å/rad step lengths) and use 2nd-order perturbation theory to compute the vibrationally averaged structure first. Then calculate the dipoles of these structures on our Ames-0 DMS. All our dipoles computed this way are higher, i.e. δ (Expt. – this work) = -0.00503D, -0.01182D, -0.00332D, -0.00446D for GS, ν_1, ν_2, and ν_3, respectively. This amounts to -0.3%, -0.7%, -0.2%, -0.3% deviations, respectively. This is not an exact comparison since the dipole of a vibrationally averaged structure is different from the vibrationally averaged dipole.

The vibrationally averaged structure for the GS, ν_1, ν_2, and ν_3 levels are $r(SO)_0$ = 1.435172 Å, 1.439009 Å, 1.434929 Å, 1.439739 Å; and $\alpha_{\angle OSO}$ = 119.344°, 119.392°, 119.517°, and 119.176°, respectively. Compared to Martin's work,[42] we find very consistent geometry changes from the equilibrium structure to the GS structure. For example, $\delta(r,\alpha) = (r,\alpha)_0 - (r,\alpha)_e$: 0.00408Å and 0.026° (this work) vs. 0.00397Å and 0.02?°.[42]

Our equilibrium rotational constants agree excellently with those reported in Morino et al.[56] $A_e/B_e/C_e$ = 2.01756/0.34556/0.29506 cm^{-1} (Expt) vs. 2.01735/0.34546/0.29495 cm^{-1} (Ames-1). The reported experimental uncertainties are less than 2-3×10^{-5} cm^{-1}. Differences between the two sets of values are as small as 1-2 × 10^{-4} cm^{-1}, or 3-6 MHz. However, in 1969 Saito reported a slightly larger A_e constant 2.01813 cm^{-1},[55] and Martin's "Best estimate" constants [42] were even larger. The results of this study suggest that the values in Morino et al.[56] could

be more reliable, though we note that equilibrium rotational constants are not direct observables, and it would be better to compare vibrationally averaged rotational constants.

The vibrationally averaged rotational constants $A/B/C$ for the $^{32}S^{16}O_2$ ground state in CDMS are 60788.550 / 10318.022 / 8799.754 MHz.[60] Our $A_0/B_0/C_0$ via 2nd-order perturbation theory are 60749.761 / 10315.501 / 8797.185 MHz, or 2.0263939 / 0.3440881 / 0.2934425 cm^{-1}. The differences, computed as (this work – CDMS), are -38.8 MHz (0.06% A_0), -2.5 MHz (0.025% B_0) and -2.5 MHz (0.03% C_0), respectively. The ground state $A_0/B_0/C_0$ of $^{34}S^{16}O_2$ reported in Lafferty et al.[51] are 1.967734 / 0.344188 / 0.292246 cm^{-1}. The corresponding values generated in this work via perturbation theory are 1.9667886 / 0.3441028 / 0.2921615 cm^{-1}, which are less by 0.00098 / 0.000085 / 0.000085 cm^{-1} or 0.05% / 0.025% / 0.03%, respectively.

Next we compare the vibrationally averaged rotational constants for the three fundamental states of $^{32}S^{16}O_2$. For ν_2=1, the CDMS A/B/C constants are 61954.816 / 10320.397 / 8783.856 MHz, and the Ames QFF 2nd-order perturbation theory constants are 61873.402 / 10318.615 / 8781.711 MHz. The differences for B/C are similar to those for ν_2=0 (GS), while the difference for A is almost doubled. The differences between the A/B/C constants for ν_1=1 and the ground state are 0.001185 cm^{-1}, -0.001676 cm^{-1}, and -0.001414 cm^{-1}, respectively, which are in nice agreement with those established in 1993 by Flaud et al [57]: +0.001082 cm^{-1}, -0.001662 cm^{-1} and -0.001412 cm^{-1}. The differences between ν_3=1 and the ground state $A/B/C$ are -0.020415 cm^{-1}, -0.001169 cm^{-1} and -0.001082 cm^{-1}, respectively. These also agree well with the Flaud et al [57] values: -0.020710 cm^{-1}, -0.001166 cm^{-1} and -0.001097 cm^{-1}. These comparisons show that the Ames-1 PES is performing very well.

Of course, another approach to obtain the vibrationally averaged $A/B/C$ for all vibrational states for the Ames-1 PES would be by fitting to the related transitions from the Ames-296K IR line list, though we have not done that here.

IV.3 Properties of Ames-1 PES: rovibrational energy levels

The comparison for rovibrational energy levels is based on matching every HITRAN or new experimental (denoted NEW-EXP) level to the closest level in the appropriate *JPS* symmetry block computed on the Ames-1 PES. This method works well and no dual matches have been found. As long as the existing assignment can satisfy the *JPS* symmetry, the specific quantum numbers $\nu_1/\nu_2/\nu_3$ and K_a/K_c are not important.

Originally there are 13 vibrational states (including the GS) of $^{32}S^{16}O_2$ in HITRAN. But $\nu_1+\nu_3$, $\nu_1+\nu_2+\nu_3$ and $3\nu_3$ rovibrational levels are excluded from our comparisons due to the ierr and multi-determination limits, see Sec.III-4. For new experimental data, the maximum multi-determination width (uncertainty) is 0.0044 cm^{-1}, so all 3959 levels of 7 new vibrational states have been included. See results in Table 2. For 12,441 J=0-80 HITRAN-based levels, the deviation varies from -0.057 cm^{-1} to 0.065 cm^{-1}, with 0.0001 cm^{-1} (mean) ± 0.0122 cm^{-1} (1σ). The total root-mean-square deviation σ_{RMS} = 0.0122 cm^{-1}.

[Table 2 Statistics for J=0-80 energy levels in HITRAN and New Expt. levels. (in cm^{-1})]

This overall agreement has led us to believe that the HITRAN data included in Table 2 are probably self-consistent. Most of the remaining energy levels excluded here have even higher K_a, e.g. for GS K_a>35 or for ν_3 K_a>33. For example, the J=34-45 and K_a=34/35 levels of the ν_3 band have much larger discrepancies: Δ(Ames-1 – HITRAN) = -0.340 cm^{-1} for the K_a=34 level, or Δ = -0.470 cm^{-1} for the K_a=35 level, with an exception Δ = 0.284 cm^{-1} at J/K_a=38/35. Our tests have concluded this is not caused by any problems in our variational VTET calculations. This strongly suggests that the K_a-extrapolation degradation in the existing spectral models needs further investigation. See Section V for more details.

It is interesting to note the HITRAN J>50/K_a=11 levels of the $\nu_1+3\nu_2$ band and $2\nu_3$ bands need to exchange their

band names to recover the energy consistency for each band. Fig.2 shows the breaks in the existing HITRAN (left, before exchange) and the smooth curves at right (after the exchange). This exchange is already included in Table 2. In addition, IR intensity tests for the related HITRAN transitions found similar breaks (not shown here).

[Fig.2 New Assignment for J > 50 / K_a=11 levels of $\nu_1+3\nu_2$ and $2\nu_3$ levels: (a) with current HITRAN band names; (b) with exchanged band names.]

In new experimental levels, only one level is confirmed as an outlier, $\nu_2+3\nu_3$ $J_{Ka,Kc}=33_{1,32}$ at 4909.9404 cm^{-1}, where the Δ(Ames-1 – Expt) = 0.315 cm^{-1}. We have consistent -0.029 cm^{-1} ~ -0.035 cm^{-1} deviations for all other $\nu_2+3\nu_3$ K_a=0/1 or J≥33 levels. So this level is excluded from the statistics in Table 2. After excluding this level, deviations for the other 3958 new experimental levels varies from -0.171 to 0.096 cm^{-1}, with -0.0191 cm^{-1} (mean) ± 0.0268 cm^{-1} (1σ) and a total σ_{RMS} = 0.0333 cm^{-1} with respect to zero. All other relatively larger deviations found with the new experimental data (i.e. Δ close to -0.17 cm^{-1} or Δ close to +0.09 cm^{-1}), are associated with the higher end of K_a. It can be reasonably explained by defects in either the Ames-1 PES or the experimental models, but further tests and or experiments will be needed to distinguish between these possibilities. In the future, we will determine whether the higher-K_a related errors can be minimized in the development of the Ames-2 PES. See Section VI for the updates coming from a new H_{eff} model.

Patterns of energy level errors along with the J, K_a and energy have been examined for both the HITRAN levels and the new experimental levels. See Fig.3 for the number of levels and σ_{RMS} for each J, K_a and 250 cm^{-1} interval.

[Fig. 3. Number of HITRAN and new experimental levels and deviations at each J, K_a and each 250 cm^{-1} interval. Solid circles and triangles are HITRAN levels, while the empty circles and triangles stand for new experiment results.]

Fig. 3 suggests the following conclusions: (1) from 0 to 4200 cm^{-1}, the J/K_a dependence of energy deviations may be further reduced in a future improved version of Ames-1 PES; (2) when extrapolated beyond 4200 cm^{-1}, Ames-1 performs very well for band origins and low J/K_a levels, while larger deviations (Ames-1 – New Expt) mainly occur for high K_a levels.

IV.4 Ames-296K IR line list for $^{32}S^{16}O_2$

IV.4.A Basics of the Ames-296K IR linelist

J=0-80 calculations for $^{32}S^{16}O_2$ only printed out all eigenstates up to 0.06 a.u. (13,168 cm^{-1}) including the zero-point energy (ZPE) 1535.6336 cm^{-1}. An initial IR line list has been generated at 296K with the purely *ab initio* DMS (Ames-0) and all J=0-80 rovibrational state wavefunctions. The converged total partition function with zero at ZPE is 6336.789 at 296K, and 6487.82 at 300K. The corresponding HITRAN partition sum at 296K is 6340.277.[58] The difference is ~0.05% and can be ignored in the intensity comparisons. In total, there are 4,094,986 transitions with intensity cutoff set to 10^{-30} cm.molecule^{-1} at 296K. However, it should be noted that this cut-off is not deep enough for IR spectral simulations >5500 cm^{-1}. Fig.4 shows the overall comparison between HITRAN and our Ames-296K IR line list, with a Gaussian convolution of 1σ = 1 cm^{-1}. The cut offs applied here are 10^{-30}, 10^{-32} and 10^{-36} cm.molecule^{-1}. The number of lines in 10^{-32} and 10^{-36} are 10,890,241 and 63,981,072. Natural isotope abundance is used in the comparison, i.e. the Ames-296K is 100% purely $^{32}S^{16}O_2$ while the HITRAN intensity values have been scaled back to 100% abundance by dividing them by 0.9457.

[Fig. 4. Compare HITRAN2012 and Ames-296K Line lists for $^{32}S^{16}O_2$. (use 100% isotope abundance)]

Ensuring the convergence of the $^{32}S^{16}O_2$ wavefunctions is the most difficult part in performing the SO_2 IR line list computation. The contracted basis sometimes fails to converge under certain conditions, which results in several false peaks in the spectra. Occasionally, computational defects affect the energies of lower states, but some do not. Experimental/HITRAN data are available only in a very limited energy region, and at limited K_a values. Hence, if a defect did not affect those HITRAN/new-experiment energy levels, we would not notice it until a simulated spectra is plotted using the already computed line list. We have endeavored to eliminate all possible defects in the Ames-296K line list, and present it as the best alternative available for bands that have yet to be measured, but it is difficult to guarantee that no noise or fake peaks exist within the millions of lines we have computed. We have found that SO_2 is even more difficult than CO_2, due in large part to the density of states.

A limitation that results from the J and energy cutoffs adopted for computation of the Ames-296K line list is that the reliability of the region above 8000 cm^{-1} is difficult to estimate. Based on experience, the region below 5500 cm^{-1} will be the most accurate and reliable. Again, based on experience, the region from 5500 to 7000 cm^{-1} will likely start off with similar accuracy as below 5500 cm^{-1}, but will degrade on going to higher energies. This degradation is likely to be band-dependent and not necessarily monotonic, but the line list should still be very useful for assigning new high-resolution experimental data, similar to what was done previously with our NH_3 and CO_2 line lists [19,22]

On the other hand, based on the comparisons we have performed, we choose to keep this section simple and basic. That is, we briefly report what have found and leave out detailed discussions for a future paper wherein we compute an upgraded IR line list. We first compare to HITRAN and CDMS, and then we show that Ames-296K based IR simulations agree very well with the recent high-resolution experimental spectra reported in Ulenikov et al. [Refs.45-49] Note that the symmetric residual $\delta(I)\% = 50\% \times (I_{Ames} / I_{obs} - I_{obs}/ I_{Ames})$ is adopted for the comparisons of IR intensities.

IV.4.B Comparison to IR transitions in HITRAN

The HITRAN2012 database includes 69,356 lines for $^{32}S^{16}O_2$ with both J_i and $J_f \leq 80$. Excluding the CDMS purely rotational transitions (12,328 at ν_2=0 and 9,007 at ν_2=1), there are 48,020 transitions for the other 11 IR bands. Table 3 presents a statistical summary of errors for each band including frequency, sum of intensity, and individual intensities. Not all the HITRAN transitions were included due to large experimental uncertainties (ierr < 4, as shown in the energy level comparisons), band name disagreement, and high end K_a levels. To avoid those discrepancies and the quantum number twisting problem we identified for a small portion of computed levels, we choose to match our computed lines to HITRAN transitions if the following criteria are met: J_i and J_f agree, parity (K_a+n_{v3}) agree, and both E_i and frequencies agree to within 0.2 cm^{-1}. This rule is not equivalent to the rules we used for energy level comparison, and all transitions related to the K_a=11 ν_1+3ν_2 and 2ν_3 levels are excluded, as well. The total number of lines included in this comparison, then is 68,965.

[Table 3. Statistical summary for 13 HITRAN bands, 130 ←000 is excluded.]

Table 3 summarize the key statistical analyses of the Ames-296K line list vs. HITRAN2012 for 13 bands. $\Delta\pm\sigma(\Delta)$ for transition wavenumbers and $\delta\%(I)\pm\sigma(\delta\%)$ for intensities are the most characteristic numbers that should

be examined. Note that detailed plots of the distribution of frequency and intensity errors are given in the EPAPS material.[Ref.53], and only a brief summary is presented here:

(1) Ames-296K intensities are systematically higher than CDMS intensities of the ν_2=0/1 purely rotational bands. See further discussion in the next section;

(2) For $A_1 \leftarrow A_1$ type transition bands, e.g. $2\nu_2 \leftarrow \nu_2$ and $2\nu_3(\leftarrow GS)$, intensity deviations $\delta(I)\%$ start from zero and bifurcate into branches with opposite K_a linear dependences;

(3) For $B_2 \leftrightarrow A_1$ type transition bands, e.g. ν_3 and $\nu_1+\nu_2+\nu_3 \leftarrow \nu_2$, $\delta(I)\%$ does not exhibit a bifurcation but monotonically drops along K_a with the negative slope proportional to the ν_3 quanta change. As a result, the worst intensity agreement in Table 3 is found for $3\nu_3(\leftarrow GS)$.

(4) The $2\nu_3$ band $\delta(I)\%$ has a wide negative tail resulting from its resonance with $\nu_1+3\nu_2$. The resonance reaches its maximum value at K_a=11 which was excluded, as its relative intensity residual $\delta(I)\%$ exceeds -400%.

(5) Based on plots of the detailed data, there is not an explicit correlation between error in the transition frequency and error in the intensity.

(6) Obvious frequency error outliers will require further investigation such as diverged $\Delta(\nu_1)$ at K_a>25, irregular $\Delta(\nu_1+\nu_3)$ at K_a>19, and $\Delta(\nu_1+\nu_2+\nu_3 \leftarrow \nu_2)$ at K_a=18.

It should be emphasized that these values do not change by more than 5% in the various dipole surface tests, from the CCSD(T)/cc-pV(Q+d)Z dipole on the Ames-1 PES grid to the CCSD(T)/aug-cc-pV(Q+d)Z dipole on a much larger grid. Least-squares fitting tests also have no observable impact on the intensity comparison results. Given the level of theory and the basis set adopted in the *ab initio* dipole calculation, it is unlikely the level of electronic structure theory used is the major source of IR intensity discrepancies.

IV.4.C Comparison to CDMS

The 528 (302) experimentally based ν_2=0 (ν_2=1) purely rotational transition lines available online at the CDMS website [59] are actually a subset of the original CDMS fitted 680 (356) lines.[60] The 528 (302) lines are given as both line frequency and uncertainty where experimentally determined. The fitted spectroscopic models are then used to extrapolate to the full CDMS database including 14754 (9808) lines. Here we compare to both the purely Expt/fitted set of 528 lines and the full CDMS, but excluding those J>80 lines. Our Ames IR line list has been re-computed at 300K, however, the partition function difference is as large as 1.2%: 6487.82 (Ames-300K) vs. 6408.32 (CDMS 300K). The CDMS value includes only two vibrational states, ν=0 (GS) and ν_2=1, in the partition function computation.

For ν_2=0, the max K_a in the purely CDMS fitted set is 23 (except for two lines at K_a'=26 and K_a'=28). Fig.5 (a) and (b) plot both frequency and intensity deviations for Ames-300K vs. the CDMS fitted set (left) and the complete CDMS set (right). The frequency deviation range $\delta(E)$ is -0.0155 – 0.0203 cm^{-1}, with mean $\delta(E) \pm \sigma_{RMS}(E)$ = 0.0012 ± 0.0045 cm^{-1}. Ames-300K reproduces the intensity of most transitions to a $\Delta(I)\%$ value in the ±5% range: the median $\Delta\%$ = -0.32%, the mean $\Delta\%$ = 0.19% and σ_{rms} ($\Delta\%$) = 1.77%. Note the partition sum difference at 300K is not included. With the partition sum adjustment included, the intensity deviation $\Delta(I)\%$ range is -4.5% – 10.7%, and the mean ± uncertainty is 1.42% ± 1.77%. When K_a rises, the ^RQ branch $\delta\%$ goes from near zero to negative, but the $\delta\%$ for most other branches slightly increases.(See EPAPS) These statistics agree with the dipole comparison result where our dipoles computed at vibrationally averaged structures agree with the experimental value to within 0.2-0.7%. Fig.6 shows how the intensity deviations depend on the ΔJ and ΔK_a quantum numbers. These differences may be partly due to the neglect of distortion corrections in the CDMS intensity predictions [61], as well as from inadequacies in the Ames-1 based calculations.

[Fig. 5 Ames-300K vs. CDMS comparison: (a) ν_2=0, the pure expt data used in CDMS fit; (b) ν_2=0, the full CDMS; (c) ν_2=1, the pure expt data used in CDMS fit; (d) ν_2=1, the full CDMS.]

[Fig. 6. Branched comparison for pure rotational band (ν_2=0) intensity discrepancy, Ames-300K vs. the pure expt data used in CDMS fit.]

The comparison to the full CDMS set where the highest K_a > 40 shows significantly larger errors, especially at higher K_a. The δ% error pattern still depends on different ΔJ and ΔK_a branches. However, it is interesting to note that both the J and K_a dependences increase with increasing ΔK_a values. This suggests that the source behind these systematic errors is probably a term associated with ΔK_a. For each ΔK_a, the P/Q branch deviations have similarly negative J dependence but the R branch deviations exhibit an opposite (positive) J dependence. The highest δ% for the existing CDMS data (>60%) occur for ΔJ=1 and ΔK_a=-3, but the steepest J or K_a dependence is found for ΔK_a=7. For those K_a>35 transitions, intensity δ% variations are still consistent with J≤35 transitions, but the frequency errors quickly rise from 0.002 cm^{-1} up to 0.10 cm^{-1}. It should be noted that the upper limit of reliable K_a for the ground state levels was estimated to be 35 in Müller and Brünken's original CDMS paper.[60]

For ν_2=1, the max K_a' in the purely CDMS fitted set is 21, and the full CDMS predicts up to K_a=39. All error patterns are very similar to ν_2=0. Frequency errors range from -0.013 cm^{-1} to 0.018 cm^{-1}, with mean ± 1σ = 0.0005 ± 0.0047 cm^{-1}. The intensity deviations Δ% are in the -3.1% – 5.3% range, with mean Δ ± $1\sigma_{RMS}(\Delta)$ = 0.9% ± 1.6%. *This clearly shows that the quantum no. twisting problem does not affect the patterns at all*. Note that the partition sum difference is already included in these deviations. Again, for the high end K_a > 33, the intensity error δ% is still consistent with other transitions while the frequency errors increase to near 0.10 cm^{-1}.

IV.4.D Simulated spectra vs. recent high-resolution experiments.

As the new experimental spectra reported in Ref.45-49 are transmittance, we only compare the overall spectra features, matching the peaks, but not quantitatively compare the absolute intensities.

Figure 7 compares $3\nu_1$ in the 3412 – 3414 cm^{-1} spectral range: experimental spectra (top black curve) reported in Ref.48 vs. an IR simulation using the Ames-296K line list with a Gaussian line width 0.002 cm^{-1}. We are satisfied with the overall agreement. The simulated spectrum is down shifted by 0.01 cm^{-1}. All the major peaks can be easily matched within 0.01-0.02 cm^{-1}. However, there are two features (black squares at 3413.05 and 3413.91 cm^{-1}) in which the experimental model did not reproduce features that were labeled as impurities.[Ref.48]. The peak at 3413.05 cm^{-1} is probably due to an impurity, but the feature at 3413.91 cm^{-1} is reproduced in our simulation as $^{P5}Q40$ of $3\nu_1$ with intensity 1.25 × 10^{-25} cm.molecule^{-1} at 3413.9136 cm^{-1}. This is very interesting, because the corresponding $^{P5}Q40$ transition frequency based on the experimental model is actually in good agreement, i.e. 3413.9084 cm^{-1}.

[Fig. 7 Ames-296K-based IR simulation (bottom red line) vs. observed $^{32}S^{16}O_2$ $3\nu_1$ *P* branch spectra (top black line, reproduced with permission from J. Mol. Spectrosc. 255, 111 (2009). Copyright 2009 Elsevier Inc.)]

A second example is the $^{32}S^{16}O_2$ $\nu_2+\nu_3$ spectra in the 1870 – 1872 cm^{-1} range (see Fig. 8). Experimental spectra was reported in Ulenikov et al.[46] Again our simulated spectra reproduce most of the main features with reasonable intensity agreement and 0.01-0.02 cm^{-1} line position errors. The missing peak at 1870.8 cm^{-1} is not $^{32}S^{16}O_2$, as both the experimental model and our IR line list do not contain the feature. There are many "grass-like" small peaks

attributed to hot-band $2\nu_2+\nu_3 \leftarrow \nu_2$ transitions, and our simulation reproduces these features.

[Fig. 8. Ames-296K-based IR simulation (bottom red line) vs. observed $^{32}S^{16}O_2$ $\nu_2+\nu_3$ spectra (top black line, reported in Ref.46), including the hot-band $2\nu_2+\nu_3 \leftarrow \nu_2$ features at right end.]

V. New Effective Hamiltonian Analysis

Very recently (while this paper was being written), Ulenikov and co-workers [62] presented their latest high-resolution IR spectroscopy measurements in the 1000-1500 cm^{-1} region together with a new Effective Hamiltonian (H_{eff}) model analysis for the ground state (GS) and three vibrational bands in the region: ν_1, ν_3 and $2\nu_2$. The J_{max} (K_a^{max}) assigned to their observed transition lines are 89(37), 109(28) and 54(9), respectively. They determined that the GS rotational parameters used in the previous literature and databases (including CDMS and HITRAN) could not reliably describe the ground state combination differences (GSCD) for those levels with K_a greater than about 26. The discrepancy between their measured and previously-modeled GSCD increased from 1.0~1.5E-4 cm^{-1} (K_a<25) to 6.05E-3 cm^{-1} (K_a=34). This was mainly attributed to the fact that the old H_{eff} model was fit from K_a^{max}=23 highly-accurate sub-mm transitions [as quoted from Ref. 62, while the CDMS website data does include two transitions with K_a'=26/28]. Therefore, Ulenikov and co-workers have developed a significantly improved fit including 78 new experimental GSCD values with J^{max}=53 and K_a^{max}=34. This new model successfully reduced the σ_{RMS} for the 78 GSCD values ($34 \geq K_a \geq 29$) from 2.69E-3 cm^{-1} to 1.1E-4 cm^{-1}. Further, the σ_{RMS} for the old 149 sub-mm experimental transitions were also reduced from 28.2 kHz to 22.5 kHz. This conclusively shows that the new effective Hamiltonian model is superior and more reliable than the previous one, i.e. the one that CDMS/HITRAN have been using and we compared to our Ames-1 PES and Ames-296K line list in the sections above. In addition, with the resonances among the three states included, 51 newly fitted parameters can successfully reproduce more than 4000 rovibrational energies which were derived from 12,131 experimental transitions of ν_1, ν_3, and $2\nu_2$ bands with σ_{RMS} around 0.0001 cm^{-1}. Thus, the known information for the ν_1 and ν_3 bands is doubled.

[Fig.9 Differences of the GS/ν_1/ν_3/$2\nu_2$ energy levels and transition frequencies between Ames (This work), New Effective Hamiltonian analysis in 2013 (see text for details), and HITRAN data (which is CDMS based): (a) and (b) show the energy level differences, (c) and (d) show the transition wavenumber differences.]

The GS levels derived from this latest H_{eff} model have been pre-screened for higher reliability by Prof. Ulenikov's group, and one set of 2173 GS levels have been kindly shared with us, with K_a^{max}=45 and J^{max}=100.[63] These GS levels are combined with 12,131 measured $\nu_1/\nu_3/2\nu_2$ transition wavenumbers to get the rovibrational energies of the associated $\nu_1/\nu_3/2\nu_2$ levels. The numbers of the derived levels are 1863(ν_1), 1628(ν_3), and 1305 ($2\nu_2$), respectively. In HITRAN2012, we find 23,504 GS and $\nu_1/\nu_3/2\nu_2$ transitions (both J_{up} and $J_{low} \leq 80$, and ierr$\geq$2) that can match with the new H_{eff} based levels, i.e. both lower and upper levels of those transitions belong to the updated set. This is the data used next for comparison in Fig.9.

There are three sets of data to compare: HITRAN2012, Ames, and New.H_{eff}.Model. We compute all three ΔE differences and include them in Fig.9, which are ΔE (New.H_{eff}.Model – HITRAN), ΔE (Ames – HITRAN), and ΔE (Ames – New.H_{eff}.Model). Plot (a) and (b) are for energy level differences, and plot (c) and (d) are for transition wavenumber differences.

It is obvious that the blue triangle (New H_{eff} vs. HITRAN) outliers and the black square (Ames vs. HITRAN) outliers are almost always close to each other, in all 4 plots (a)-(d). As shown in plot (a) and (b), the discrepancies

between Ames and the new H_{eff} levels are insignificant until E > 3500 cm^{-1} and K_a > 42. Those Ames-HITRAN large discrepancy outliers at 2000 cm^{-1} and 2500~3500 cm^{-1} do not exist in the Ames-New.H_{eff}.Model comparison.

Examining plot (b), the agreement between Ames and the new H_{eff} (red circles) at high K_a is much better than that between Ames and HITRAN. Actually, ΔEs at K_a=43 are now reduced from 0.439 cm^{-1} (Ames – HITRAN) to 0.040 cm^{-1} (Ames – new H_{eff}). Furthermore, only 6 K_a=44-45 levels have ΔE(Ames – new H_{eff}) > 0.10 cm^{-1} and ΔE^{max} = 0.194 cm^{-1}, as shown at the right end of plot (b). On the other hand, the most negative ΔE(Ames – new H_{eff}) for energy levels appear around –0.05 cm^{-1} with K_a=0/1 and J close to 80. The corresponding ΔE(Ames – HITRAN) are similar for those energy levels. However, the most negative ΔE(Ames – HITRAN) were -0.06 ~ -0.14 cm^{-1} for the GS and ν_1 at K_a=31/32, J=31-40. Most of these larger deviations have been significantly reduced, e.g. the new ΔEs at K_a=31 are -0.009 cm^{-1} for the GS and -0.039 – -0.047 cm^{-1} for ν_1.

In short, the new H_{eff} model and our work show remarkable similarities in the wide range of K_a=23-42. This clearly proves the reliability and higher internal consistency of our "High-resolution Experimental Data + Best Theory" approach. As we have stated before, the most valuable part of our approach is to provide "truly reliable" predictions (and alternatives) for those unknown or hard-to-measure / analyze spectra. Without knowing any new experimental data, our Ames-1 PES based predictions at K_a > 30 were much more reliable than any other pre-existing models.

In plot (d), one can see that at around K_a=30 both the ΔE(Ames – new H_{eff}) and the ΔE(Ames – HITRAN) were negative, while ΔE(new H_{eff} – HITRAN) are nearly zero. This may suggest the discrepancy source could be mainly on our end, probably on the data we included in the Ames-1 PES refinement. This is part of the planned improvements in a future Ames-2 PES refinement, which definitely will utilize these new H_{eff} based analysis results.

Based on the Fig.9 (a)-(d) plots, we estimate the new H_{eff} model GS levels reliably extrapolate to K_a=43-45 (for an energy uncertainty less than 0.01-0.02 cm^{-1}). Our Ames-1 PES based predictions at higher K_a region can provide useful reference for future laboratory work / model development and can be further refined when laboratory data become available.

Finally, we consider this a perfect example for a long-time standing question about the reliability of extrapolating to higher quantum number values for H_{eff} based experimental models versus theoretical or variational computations. Our basic conclusion is that H_{eff} models are able to maintain higher (1-3 orders of magnitude) accuracy in the range of accurately fitted reliable data, however theoretical line lists yield better consistency and reliability for regions far above the H_{eff} data region. For both the old and new H_{eff} models of $^{32}S^{16}O_2$, the problematic point for K_a is about 10 – 15 above their respective K_a^{max}. As the new H_{eff} model has substantially improved the accuracy at high K_a, all other experimental bands and models should probably be re-analyzed before the next HITRAN or CDMS update. However, it should be noted that the intensity discrepancies between the Ames-296 line list and the full CDMS line lists still require further investigation.

VI. Summary and future work

In this present study, we compute an *ab initio* PES for SO_2, refine it using selected HITRAN rovibrational energy levels, and then compute an initial $^{32}S^{16}O_2$ IR line list which should significantly improve the ability for astronomers to remove the $^{32}S^{16}O_2$ "weeds" from astronomically observed spectral data. The initial IR line list (Ames-296K) is computed using the refined PES together with an unadjusted purely *ab initio* CCSD(T)/ aug-cc-pV(Q+d)Z dipole moment surface. The Ames-1 PES predictions for both interpolated and extrapolated bands are compared to recent experiments and have shown satisfactory accuracy and reliability. When compared to the HITRAN and CDMS databases, most errors have systematic patterns and probably can be tracked down to one (or a few) K_a related terms in

either our computations or especially the experimental models for high K_a. In some cases, the linear correlation between the K_a, J and discrepancies depends on ΔJ and ΔK_a. However, because they are very systematic, we believe the ~0.02 cm^{-1} and ~10% deviations for line positions and line intensities are adequate to detect certain outliers or defects in existing models, and in fact comparison to a very recent study where a new effective Hamiltonian model has been developed [62] supports that assertion for line positions. The energy levels computed using the Ames-1 PES and the Ames-296K line list are expected to facilitate future IR analyses for both missing bands below 4300 cm^{-1} and higher energy bands beyond 6000 cm^{-1}, as well as for $^{34}S^{16}O_2$.

In the future, we plan to make the following improvements: (1) incorporate Ulenikov *et al's* [Refs.45-49,62] results to achieve 0.01-0.02 cm^{-1} accuracy for everything below 6000 cm^{-1} and also extend the prediction reliability at higher energies; (2) compute a $^{34}S^{16}O_2$ IR line list;[64] (3) investigate the source of intensity discrepancies when compared to the CDMS database; (4) include diagonal Born-Oppenheimer corrections (DBOC) for energy levels and line lists of $^{17/18}O$ isotopologues; (5) compute and include the non-adiabatic corrections which might help the high-end K_a agreement; (6) further improve the convergence of variational CI calculations to extend the IR line list beyond 10,000 cm^{-1}, and J>80, for higher temperature IR simulations. Additionally, we may carry out an independent study focusing on the far-infrared region to yield microwave spectra for $^{32/34}S^{16}O_2$, with better than 3-6 MHz and 5-10% accuracy for line positions and intensity, respectively.

The Ames-1 PES, the *ab initio* dipole surface, and the Ames-296K line list can be downloaded from supplementary EPAPS material, [53] or available upon request to authors.

Acknowledgement

We gratefully acknowledge funding support from the NASA Grants 08-APRA08-0050 and 10-APRA10-0096. XH also thanks the support from the NASA/SETI Institute Cooperative Agreements NNX09AI49A and NNX12AG96A. We sincerely appreciate the kind permission from Dr. Oleg Ulenikov (Tomsk State U) and Dr. Veli-Matti Horneman (OULU) for sharing their published experimental spectra and the latest GS level set derived from their new Effective Hamiltonian Model published in 2013. Dr. Holger Müller (Cologne), Dr. Brian Drouin (JPL), and Professor Jonathan Tennyson (UCL) are thanked for helpful discussions.

Tables

Table 1. $^{32/34}S^{16}O_2$ band origins up to 5165 cm^{-1}, computed on Ames-1 PES and compared with available experimental data. Note: new $^{32}S^{16}O_2$ band origins in Refs.45-49 and $^{34}S^{16}O_2$ band origins in Refs.51-52 were not included in the Ames-1 empirical refinement.

	$^{32}S^{16}O_2$			$^{34}S^{16}O_2$		
Band/cm^{-1}	**Expt.[&#]**	**This work**	**Calc-Expt**	**Expt[$]**	**This work**	**Calc-Expt**
A'-symmetry						
ZPE		1535.6336			1521.1034	
ν_2	517.8726	517.8708	-0.0018	513.5187	513.5337	+0.0150
$2\nu_2$	1035.1264	1035.1121	-0.0143	1026.4555	1026.4359	-0.0196
ν_1	1151.7130	1151.7115	-0.0015	1144.4786	1144.4881	+0.0095
$3\nu_2$	1551.7553[b]	1551.7447	-0.0106	1538.7202	1538.7272	**+0.0070**
$\nu_1+\nu_2$	1666.3348	1666.3226	-0.0122	1654.8290	1654.8172	-0.0118
$4\nu_2$	*(2066.9)*	2067.7815			2050.4207	
$\nu_1+2\nu_2$	2180.3312[b]	2180.3074	-0.0238		2164.5172	
$2\nu_1$	2295.8083	2295.8146	0.0063		2281.5072	
$5\nu_2$	*(2582.3)*	2583.2272			2561.5218	
$\nu_1+3\nu_2$	2693.6348[a] 2693.7279[c]	2693.6859	0.0511 -0.0420		2673.6078	
$2\nu_3$	2713.3826	2713.3862	0.0036	2679.8009	2679.7922	-0.0087
$2\nu_1+\nu_2$	2807.1881[c]	2807.1715	-0.0166		2788.6360	
$6\nu_2$	*(3095.6*)	3098.0789			3072.0285	
$\nu_1+4\nu_2$	*(3205.8*)	3206.4707			3182.1012	
$\nu_2+2\nu_3$	3222.9725[c]	3222.9510	-0.0215		3185.2447	
$2\nu_1+2\nu_2$	*(3318.1*)	3317.9021			3295.1355	
$3\nu_1$	3432.2877[d]	3432.2839	-0.0038		3411.0307	
$7\nu_2$	*(3608.9)*	3612.3254			3581.9311	
$\nu_1+5\nu_2$	*(3717.4)*	3718.6665			3689.9829	
$2\nu_2+2\nu_3$	*(3730.9)*	3731.9384			3690.1352	
$2\nu_1+3\nu_2$	*(3828.1)*	3828.0259			3801.0247	
$\nu_1+2\nu_3$	*(3923.8)*	3837.5893			3797.0989	
$3\nu_1+\nu_2$	*(3939.9)*	3940.3920			3914.9634	
$8\nu_2$	*(4121.3)*	4125.9477			4091.2121	
$\nu_1+6\nu_2$	*(4228.1)*	4230.2707			4197.3139	
$3\nu_2+2\nu_3$	*(4241.5)*	4240.3554			4194.4079	
$2\nu_1+4\nu_2$	*(4342.7)*	4337.5544			4306.3153	
$\nu_1+\nu_2+2\nu_3$	*(4344.3)*	4343.7922			4299.2482	
$3\nu_1+2\nu_2$	*(4446.9)*	4447.8721			4418.2651	
$4\nu_1$	*(4560.1)*	4561.1041			4533.0415	
$9\nu_2$	*(4632.9)*	4638.9188			4599.8466	
$\nu_1+7\nu_2$	*(4738.1)*	4741.2725			4704.0195	
$4\nu_2+2\nu_3$	*(4748.3)*	4748.2031			4698.1296	
$2\nu_1+5\nu_2$	*(4845.0)*	4846.4909			4811.0122	
$\nu_1+2\nu_2+2\nu_3$	*(4848.1)*	4849.4206			4800.8153	
$2\nu_1+2\nu_3$	*(4953.8)*	4953.5546			4906.3149	
$3\nu_1+3\nu_2$	*(4955.1)*	4954.7439			4920.9537	
$4\nu_1+\nu_2$	*(5066.7)*	5065.9680			5033.7814	
$10\nu_2$	*(5143.8)*	5151.2137			5107.8021	
A" symmetry						
ν_3	1362.0603	1362.0585	-0.0018	1345.0946	1345.0827	-0.0119
$\nu_2+\nu_3$	1875.7975	1875.7913	-0.0062	1854.6104	1854.5901	-0.0203

$2\nu_2+\nu_3$	2388.9155	2388.9226	0.0071		2363.4927	
$\nu_1+\nu_3$	2499.8700	2499.8906	0.0206	2475.8280	2475.8502	+0.0222
$3\nu_2+\nu_3$	(n/a)	2901.4657			2871.8039	
$\nu_1+\nu_2+\nu_3$	3010.3178	3010.3149	-0.0029	2982.1186	2982.1057	-0.0129
$4\nu_2+\nu_3$	*(3413.0)*	3414.4264			3379.5302	
$\nu_1+2\nu_2+\nu_3$	*(3520.2)*	3520.1389			3487.7569	
$2\nu_1+\nu_3$	3629.7619	3629.7874	0.0255	3598.7739	3598.8226	+0.0487
$5\nu_2+\nu_3$	*(3923.8)*	3924.8035			3886.6711	
$\nu_1+3\nu_2+\nu_3$	4029.3903	4029.3743	-0.0160		3992.8156	
$3\nu_3$	4054.0012	4054.0243	0.0231		4004.1621	
$2\nu_1+\nu_2+\nu_3$	4136.9341[e]	4136.9158	-0.0183		4101.8359	
$6\nu_2+\nu_3$	*(4433.9)*	4435.5888			4393.2193	
$\nu_1+4\nu_2+\nu_3$	*(4537.6)*	4538.0261			4497.2867	
$\nu_2+3\nu_3$	4559.4340[e]	4559.4025	-0.0315		4505.5413	
$2\nu_1+2\nu_2+\nu_3$	*(4643.5)*	4643.4436			4604.2444	
$3\nu_1+\nu_3$	4751.7169[a]	4751.6997	-0.0172		4713.9476	
$7\nu_2+\nu_3$	*(4943.3)*	4945.7665			4899.1607	
$\nu_1+5\nu_2+\nu_3$	*(5045.2)*	5046.0924			5001.1685	
$2\nu_2+3\nu_3$	*(5064.9)*	5064.2215			5006.3565	
$2\nu_1+3\nu_2+\nu_3$	*(5149.3)*	5149.3807			5106.0575	
$\nu_1+3\nu_3$	5164.8507[*]	5164.8370	-0.0137		5108.2558	

[&] $^{32}S^{16}O_2$ High-res Expt and model values were taken from [a] Ref.45 and references therein; [b] Ref.46; [c] Ref.47 ; [d] Ref.48 (2009); [e] Ref.49;

[$] $^{34}S^{16}O_2$ High-res Expt and modeled values from Ref.45, while the data was traced back to Ref.51 and Ref.52.

[#] Low-res modeled values (italic in parentheses) from Ref.39, which included 31 "observed" states, and 84 states derived from Dunham expansion formula and parameters given in Ref.40.

Table 2 Statistics for J=0-80 energy levels in HITRAN and New Expt levels. (in cm^{-1})

ν_1 ν_2 ν_3	E_min	E_max	J_{min}	J_{max}	K_a^{min}	K_a^{max}	No.	Δ_{min}	Δ_{max}	σ_{RMS}
HITRAN										
0 0 0	1.912	3958.558	1	80	0	35	2217	-0.057	0.025	0.009
0 0 1	1362.696	4025.577	1	80	0	33	1958	-0.050	0.037	0.010
0 0 2	2713.383	4436.386	0	76	0	23	1092	-0.031	0.034	0.010
0 1 0	517.872	3720.194	0	80	0	29	1942	-0.034	0.065	0.016
0 2 0	1035.126	2296.506	0	62	0	20	894	-0.019	0.032	0.009
0 3 0	1553.654	2237.936	1	45	0	17	502	-0.049	0.009	0.010
1 0 0	1151.713	3301.518	0	80	0	32	1606	-0.051	0.023	0.011
1 1 0	1666.335	3080.041	0	45	0	21	758	-0.021	0.007	0.007
0 1 1	1876.432	3964.383	1	70	0	25	1425	-0.039	0.065	0.018
1 3 0	2955.938	3789.613	11	57	11	11	47	0.023	0.052	0.042
Total	**1.912**	**4436.386**	**0**	**80**	**0**	**35**	**12441**	**-0.057**	**0.065**	**0.0122**
New Expt										
0 1 2	3224.869	3976.472	2	49	0	13	386	-0.035	0.005	0.021
0 1 3	4563.210	5071.748	3	35	0	10	182	-0.050	-0.014	0.034
1 0 3	5165.479	5944.312	1	51	0	16	473	-0.121	0.065	0.037
2 1 0	2809.081	3418.350	2	43	0	17	438	-0.034	0.002	0.016
2 1 1	4148.472	4519.131	4	26	1	11	115	-0.047	-0.016	0.029
3 0 0	3434.172	4782.933	1	66	0	24	885	-0.172	0.096	0.046
3 0 1	4752.344	5590.652	1	53	0	16	478	-0.159	0.042	0.047
Total	**2809.081**	**5944.312**	**1**	**66**	**0**	**24**	**3958**	**-0.172**	**0.096**	**0.0333**

Table 3. Statistical summary for 13 HITRAN bands, 130 ←000 is excluded.

Band in HITRAN	J_f	K_a	E_{min}	E_{max}	No.	Freq Δ_{min}	Freq Δ_{max}	Freq Δ_{mean}	Freq $\pm\sigma(\Delta)$	Sum-Int HITRAN	*Sum-Int* δ	Int δ_{min}	Int δ_{max}	Int δ_{AVG}	Int $\pm\sigma(\delta)$
000←000	0-80	0-42	0.0	265.9	12291	-0.026	0.109	0.003	0.010	2.208E-18	*2.3%*	-11.1%	64.2%	10.1%	11.2%
010←010	0-80	0-40	0.0	201.9	9007	-0.032	0.130	0.001	0.009	1.779E-19	*2.4%*	-5.4%	34.6%	5.8%	6.0%
010←000	0-70	0-26	436.6	645.6	5916	-0.024	0.037	0.001	0.010	3.707E-18	*-2.1%*	-55.1%	32.9%	-3.3%	18.9%
020←010	0-62	0-21	446.4	622.1	3727	-0.019	0.016	-0.006	0.006	5.770E-19	*-2.6%*	-44.8%	28.1%	-3.1%	16.2%
030←020	1-46	0-17	463.1	598.3	1532	-0.032	0.017	0.006	0.008	5.588E-20	*-3.3%*	-35.5%	20.3%	-3.7%	12.6%
100←000	0-80	0-32	1031.0	1273.2	8256	-0.038	0.056	-0.002	0.005	3.322E-18	*3.0%*	-47.8%	28.7%	0.7%	11.1%
110←010	0-46	0-22	1047.9	1243.8	4043	-0.026	0.019	-0.005	0.006	2.506E-19	*3.1%*	-81.1%	21.5%	0.3%	17.9%
001←000	0-80	0-33	1298.0	1405.7	5427	-0.013	0.025	0.000	0.004	2.573E-17	*2.3%*	-44.8%	8.4%	-3.7%	6.7%
011←010	0-71	0-25	1302.1	1397.0	3948	-0.018	0.049	-0.001	0.009	2.022E-18	*3.8%*	-20.9%	30.0%	-0.3%	6.7%
101←000	0-80	0-24	2433.2	2533.2	4029	-0.084	0.110	0.009	0.022	5.434E-19	*-6.4%*	-52.8%	15.3%	-11.0%	5.2%
111←010	0-61	0-21	2441.2	2521.1	2733	-0.144	0.017	-0.009	0.014	4.239E-20	*-5.2%*	-36.9%	-1.6%	-8.2%	4.1%
002←000	0-76	0-24[&]	2599.1	2787.9	4400	-0.042	0.011	0.003	0.008	3.827E-21	*-12.4%*	-96.6%	6.24%	-16.3%	11.1%
003←000	0-77	0-25	3985.2	4092.9	3656	-0.060	0.064	0.011	0.024	1.546E-21	*-19.2%*	-102.7%	15.1%	-37.7%	21.5%

[&] K_a=11 excluded.

Figure Captions and Figures

[Fig.1 Accuracy of Ames-1 PES: $^{32}S^{16}O_2$ and $^{34}S^{16}O_2$ band origins.]

[Fig.2 New Assignment for J > 50 / K_a=11 levels of $\nu_1+3\nu_2$ and $2\nu_3$ levels: (a) with current HITRAN band names; (b) with exchanged band names.]

[Fig.3 Number of HITRAN and new experimental levels and deviations at each *J*, *K*a and each 250 cm^{-1} interval. Solid circles and triangles are HITRAN levels, while the empty circles and triangles stand for new experiment results. (Refs.45-49)]

[Fig. 4. Compare HITRAN2012 and Ames-296K Line lists for $^{32}S^{16}O_2$. (use 100% isotope abundance)]

[Fig. 5 Ames-300K vs. CDMS comparison: (a) ν_2=0, the pure expt data used in CDMS fit; (b) ν_2=0, the full CDMS; (c) ν_2=1, the pure expt data used in CDMS fit; (d) ν_2=1, the full CDMS.]

[Fig. 6. Branched comparison for pure rotational band (ν_2=0) intensity discrepancy, Ames-300K vs. the pure expt data used in CDMS fit.]

[Fig. 7. Ames-296K-based IR simulation (bottom red line) vs. observed $^{32}S^{16}O_2$ $3\nu_1$ *P* branch spectra (top black line, reproduced with permission from J. Mol. Spectrosc. 255, 111 (2009). Copyright 2009 Elsevier Inc.)]

[Fig. 8. Ames-296K-based IR simulation (bottom red line) vs. observed $^{32}S^{16}O_2$ $\nu_2+\nu_3$ spectra (top black line, reported in Ref.46), including the hot-band $2\nu_2+\nu_3 \leftarrow \nu_2$ features at right end.]

[Fig.9 Differences of the GS/ν_1/ν_3/$2\nu_2$ energy levels and transition frequencies between Ames (This work), New Effective Hamiltonian analysis in 2013 (see text for details), and HITRAN data (which is CDMS based): (a) and (b) show the energy level differences, (c) and (d) show the transition wavenumber differences.]

References

[1] S. Martin, J. Martin-Pintado, R. Mauersberger, C. Henkel, and S. Garcia-Burillo, "Sulfur Chemistry and Isotopic Ratios in the Starburst Galaxy NGC 253", Astrophys. J. **620**, 210 (2005).

[2] L.M. Ziurys, "The Chemistry in circumstellar envelopes of evolved stars: following the origin of the elements to the origin of life", PNAS **103**, 12274 (2006).

[3] E. Klisch, P. Schilke, S.P. Belov, and G. Winnewisser, "$^{33}SO_2$: Interstellar identification and Laboratory Measurements", J. Mol. Spectrosc. **186**, 314 (1997).

[4] R.M. Nelson, A.L. Lane, D.L. Matson, F.P. Fanale, D.B. Nash, and T.V. Johnson, "Longitudinal distribution of SO_2 on Io", Science **210**, 7784 (1980).

[5] S. Martin, R. Mauersberger, J. Martin-Pintado, S. Garcia-Burillo, and C. Henkel, "First detections of extragalactic SO_2, NS and NO", Astron. Astrophys. **411**, L465 (2003).

[6] F.F.S. van der Tak, A.M.S. Boonman, R. Braakman, and E.F. van Dishoeck, "Sulfur chemistry in the envelopes of massive young stars", Astron. Astrophys. **412**, 133 (2003).

[7] C. Visscher, K. Lodders, and B. Fegley Jr., "Atmospheric chemistry in giant planets, brown dwarfs, and low-mass dwarf stars. II. Sulfur and Phosphorus", Astrophys. J. **648**, 1181 (2006).

[8] P. Schilke, D.J. Benford, T.R. Hunter, D.C. Lis, and T.G. Philips "A line Survery of Orion-KL from 607 to 725 GHz", Astrophys. J. Supp. Ser. **132**, 281 (2001).

[9] N.R. Crockett, E.A. Bergin, S. Wang, D.C. Lis, T.A. Bell et al. "Herschel Observations of Extra-Ordinary Sources (HEXOS): The Terahertz spectrum of Orion KL seen at high spectral resolution" Astron. Astrophys. **521**, L21 (2010).

[10] A. Belloche, H.S.P. Müller, K.M. Menten, P. Schilke, and C. Comito "Complex organic molecules in the interstellar medium: IRAM 30m line survey of Sagittarius B2(N) and (M)", Astron. Astropys. **559**, A47 (2013).

[11] N.R. Crockett, Thesis (PhD),"*Analysis of the Herschel/HIFI 1.2 THz Wide Spectral Survey of the Orion Kleinmann-Low Nebula*", University of Michigan, 192 pages, 2013.

[12] M. Kama, A. López-Sepulcre, C. Dominik, C. Ceccarelli, A. Fuente, E. Caux, et al. "*The Herschel/HIFI spectral survey of OMC-2 FIR 4 (CHESS):An overview of the 480 to 1902 GHz range*" Astron. Astrophys. **556**, A57 (2013).

[13] *The Workshop on Laboratory Spectroscopy in Support of HERSCHEL, SOFIA and ALMA*, Padadena, CA, Oct.19-20, 2006.

[14] H. Partridge H and D.W. Schwenke, "*The determination of an accurate isotope dependent potential energy surface for water from extensive ab initio calculations and experimental data*", *J. Chem. Phys.* **106**, 4618-4639 (1997).

[15] O. L. Polyansky, A. G. Császár, S. V. Shirin, N. F. Zobov, P. Barletta, J. Tennyson, D. W. Schwenke, and P. J. Knowles, *Science* **299**, 539 (2003).

[16] X. Huang, D. W. Schwenke, and T. J. Lee, *J. Chem. Phys.* **129**, 214304 (2008).

[17] X. Huang, D. W. Schwenke, and T. J. Lee, *J. Chem. Phys.* **134**, 044320 (2011).

[18] X. Huang, D. W. Schwenke, and T. J. Lee, *J. Chem. Phys.* **134**, 044321 (2011).

[19] K. Sung, L.R. Brown, X. Huang, D.W. Schwenke, T.J. Lee, S.L. Coy, and K.K. Lehmann, *Extended line positions, intensities, empirical lower state energies and quantum assignments of NH_3 from 6300 to 7000 cm^{-1}*, J. Quant. Spectrosc. Radiat. Transfer **113**, 1066-1083 (2012).

[20] S. N. Yurchenko, R. J. Barber, J. Tennyson, "A variationally computed line list for hot NH_3", *Monthly Notices of the Royal Astronomical Society* **413**, 1828-1834 (2011)

[21] X. Huang, D.W. Schwenke, S.A. Tashkun, and T.J. Lee, "*An isotopic-independent highly accurate potential energy surface for CO2 isotopologues and an initial $^{12}C^{16}O_2$ infrared line list*", *J. Chem. Phys.* **136**, 124311 (2012).

[22] X. Huang, R.S. Freedman, S.A. Tashkun, D.W. Schwenke, and T.J. Lee, "Semi-empirical $^{12}C^{16}O_2$ IR line lists for simulations up to 1500 K and 20,000 cm^{-1}" *J. Quant. Spectrosc. Radiat. Transfer* **130**, 134-146 (2013)

[23] Petrova TM, Solodov AM, Solodov AA, Lyulin OM, Tashkun SA, Perevalov VI, "*Measurements of $^{12}C^{16}O_2$ line parameters in the 8790-8860, 9340-9650 and 11430-11505 cm^{-1} regions by means of Fourier transform spectroscopy*" , J. Quant. Spectrosc. Radiat. Transfer **124**, 21-27 (2013).

[24] L.S. Rothman, et al. *The HITRAN 2008 molecular spectroscopic database*, J. Quant. Spectrosc. Radiat. Trans. **110**, 533-572 (2009).

[25] L.S. Rothman, et al. *The HITRAN 2012 molecular spectroscopic database*, J. Quant. Spectrosc. Radiat. Trans. **130**, 4-50 (2013).

[26] J. Tennyson and S.N. Yurchenko *Mon. Not. R. Astron. Soc*. **425**, 21-33 (2012)

[27] EChO Mission Candiate website: http://sci.esa.int/echo/

[28] D. W. Schwenke, and H. Partridge, *J. Chem. Phys.* **113**, 6592 (2000).

[29] R. J. Barber, J. Tennyson, G. J. Harris, R. N. Tolchenov, "A high-accuracy computed water line list", *Monthly Notices of the Royal Astronomical Society* **368**, 1087-1094 (2006).

[30] D. W. Schwenke, *J. Phys. Chem.* **100**, 2867 (1996).

[31] K. Raghavachari, G.W. Trucks., J.A. Pople, M. Head-Gordon, Chem. Phys. Lett. **157**, 479-483 (1989).

[32] T.H. Dunning, Jr., J. Chem. Phys. **90**, 1007 (1989).

[33] D.E. Woon and T.H. Dunning, Jr. J. Chem. Phys. **98**, 1358 (1993).

[34] R.A. Kendall, T.H. Dunning, Jr., R.J. Harrison, J. Chem. Phys. **96**, 6796–6806 (1992).

[35] T.H. Dunning, Jr., K.A. Peterson, A.K. Wilson, J. Chem. Phys. **114**, 9244 (2001).

[36] K.A. Peterson and T.H. Dunning, Jr., J.Chem.Phys. **117**, 10548 (2002).

[37] M. Douglas, and N. Kroll, Ann. Phys. **82**, 89 (1974).

[38] J.M.L. Martin, and P.R. Taylor, Chem. Phys. Lett. **225**, 473 (1994).

[39] A.J.C. Varandas, S.P.J. Rodrigues, Spectrochimica Acta Part A **58** (2002) 629-647.

[40] R.D. Shelton, A. H. Nielsen and W.H.Fletcher, JCP 21, 2178 (1953).

[41] J. M. L. Martin and T. J. Lee, *Chem. Phys. Lett.* **258**, 136 (1996)

[42] J.M.L. Martin, "Basis set convergence study of the atomization energy, geometry, and anharmonic force field of SO2: The importance of inner polarization functions" J. Chem. Phys. **108**, 2791 (1998).

[43] X. Huang, B.J. Braams, J.M.Bowman, *J. Chem. Phys.* **122**, 044308 (2005).

[44] (a) H. S. P. Müller, F. Schlöder, J. Stutzki, and G. Winnewisser, J. Mol. Struct. **742**, 215–227 (2005); (b) H. S. P. Müller, S. Thorwirth, D. A. Roth, and G. Winnewisser, Astron. Astrophys. **370**, L49–L52 (2001).

[45] O.N. Ulenikov, E.S. Bekhtereva, S. Alanko, V.-M. Horneman, O.V. Gromova, C. Leroy "*On the high resolution spectroscopy and intramolecular potential function of SO_2*" J. Mol. Spectrosc. **257**, 137-156 (2009), and references therein.

[46] O.N. Ulenikov, O.V. Gromova, E.S. Bekhtereva, I.B. Bolotova, C. Leroy, V.-M. Horneman, S. Alanko, "*High resolution study of the $v_1+2v_2 \leftarrow v_2$ and $2v_2+v_3 \leftarrow v_2$ "hot" bands and ro-vibrational re-analysis of the $v_1+v_2/v_2+v_3/3v_2$ polyad of the $^{32}SO_2$ molecule*" J. Quant. Spectrosc. Radiat. Trans. **112**, 486-512 (2011).

[47] O.N. Ulenikov, O.V. Gromova, E.S. Bekhtereva, I.B. Bolotova, I.A. Konov, V.-M. Horneman, C. Leroy, "*High resolution analysis of the SO2 spectrum in the 2600–View the MathML source region: 2v3, $v_2+2v_3 \leftarrow v_2$ and $2v_1+v_2$ bands*" J. Quant. Spectrosc. Radiat. Trans. **113**, 500-517 (2012).

[48] O.N. Ulenikov, E.S. Bekhtereva, V.-M. Horneman, S. Alanko, O.V. Gromova "*High resolution study of the $3v_1$ band of SO_2*" J. Mol. Spectrosc. **255**, 111-121 (2009).

[49] O.N. Ulenikov, E.S. Bekhtereva, O.V. Gromova, S. Alanko, V.-M. Horneman & C. Leroy "*Analysis of highly excited 'hot' bands in the SO_2 molecule: $v_2 + 3v_3 \leftarrow v_2$ and $2v_1 + v_2 + v_3 \leftarrow v_2$*" Mol. Phys. **108**, 1253-1261 (2010).

[50] D. W. Schwenke, *Comp. Phys. Commun.* **70**, 1 (1992).

[51] W.J. Lafferty, J.-M. Flaud, R.L. Sams, El Hadji Abib Ngom, "High resolution analysis of the rotational levels of the (0 0 0), (0 1 0), (1 0 0), (0 0 1), (0 2 0), (1 1 0) and (0 1 1) vibrational states of $^{34}S^{16}O_2$" J. Mol. Spectrosc. **252**, 72 (2008).

[52] W.J. Lafferty, J.-M. Flaud, El Hadji Abib Ngom, R.L. Sams, "$^{34}S^{16}O_2$: High-resolution analysis of the (0 3 0), (1 0 1), (1 1 1), (0 0 2) and (2 0 1) vibrational states; determination of equilibrium rotational constants for sulfur dioxide and anharmonic vibrational constants" J. Mol. Spectrosc. **253**, 51 (2009).

[53] See supplementary materials at EPAPS Link for Ames-1 PES,DMS-N1,Ames-296K Line List and comparison with HITRAN data and recent experiments.

[54] D. Patel, D. Margolese, and T. R. Dykea, "*Electric dipole moment of SO_2 in ground and excited vibrational states*" J. Chem. Phys. **70**, 2740 (1979).

[55] S. Saito, "*Microwave spectrum of sulfur dioxide in doubly excited vibrational states and determination of the γ constants*" J. Mol. Spectrosc. **30**, 1 (1969).

[56] Y. Morino,Y. Kikuchi, S. Saito, E. Hirota, "Equilibrium structure and potential function of sulfur dioxide from the microwave spectrum in the excited vibrational state" J. Mol. Spectrosc. **13**, 95 (1964).

[57] J.M. Flaud, A. Perrin, L.M. Salah, W.J. Lafferty, G. Guelachvili, "A Reanalysis of the (010), (020), (100), and (001) Rotational Levels of $^{32}S^{16}O_2$", J. Mol. Spectrosc. **160**, 272 (1993).

[58] J. Fisher, R.R. Gamache, A. Goldman, L.S. Rothman, A. Perrin J. Quant. Spectrosc. Radiat. Trans. **82**, 401-412 (2003).

[59] The CDMS Catalog, http://www.astro.uni-koeln.de/cdms/entries

[60] H. S. P. Müller and S. Brünken, J. Mol. Spectrosc., **232**, 213 (2005), and references therein.

[61] H. S. P. Müller, personal communication (2013).

[62] O.N. Ulenikov, G.A. Onopenko, O.V.Gromova, E.S. Bekhtereva, and V.-M. Horneman J. Quant. Spectrosc. Radiat. Trans. **130**, 220-232 (2013).

[63] O.N. Ulenikov, personal communication. (2013).

[64] X. Huang, D.W. Schwenke, and Timothy. J. Lee, in preparation.

Fig.1 Accuracy of Ames-1 PES: $^{32}S^{16}O_2$ and $^{34}S^{16}O_2$ band origins.

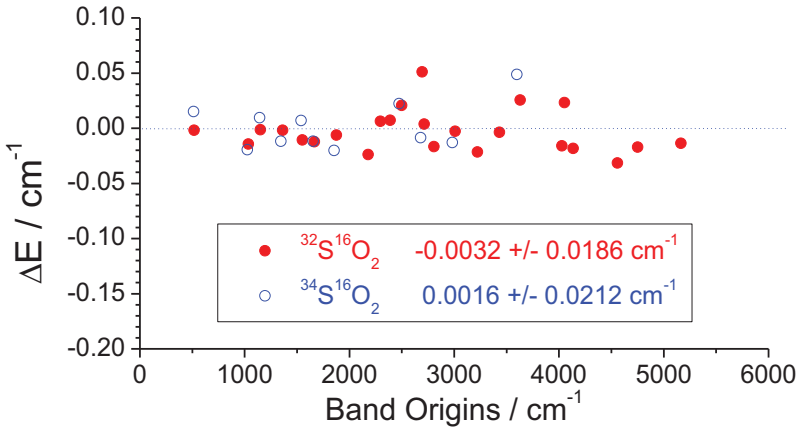

Fig.2 New Assignment for J > 50 / K_a=11 levels of $\nu_1+3\nu_2$ and $2\nu_3$ levels: (a) with current HITRAN band names; (b) with exchanged band names.

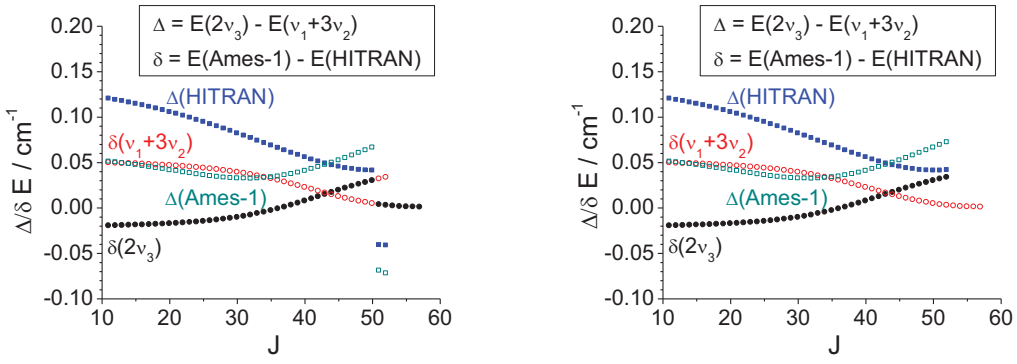

(a) (b)

Fig.3 Number of HITRAN and new experimental levels and deviations at each *J*, *K*a and each 250 cm^{-1} interval. Solid circles and triangles are HITRAN levels, while the empty circles and triangles stand for new experiment results.

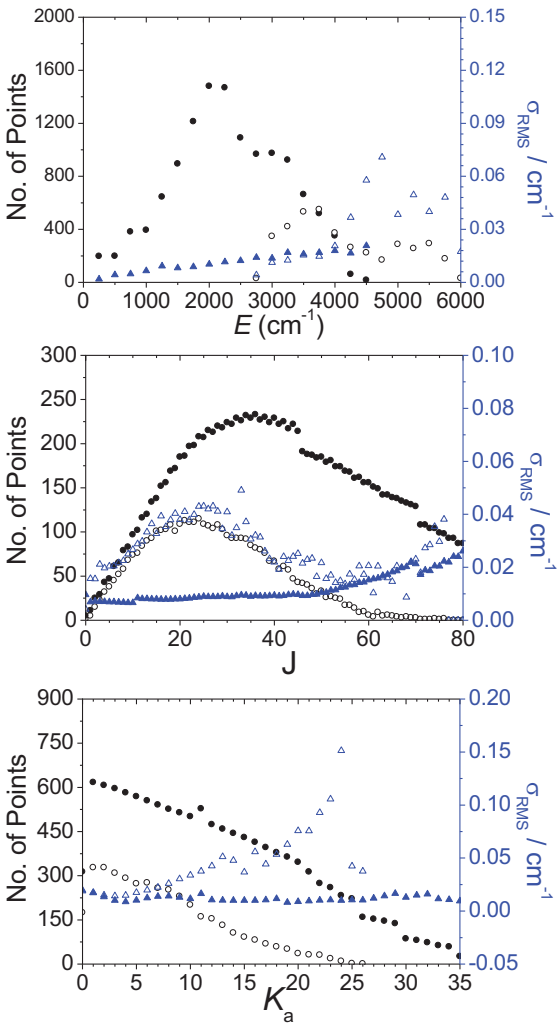

Fig. 4. Compare HITRAN2012 and Ames-296K Line lists for $^{32}S^{16}O_2$. (use 100% isotope abundance)

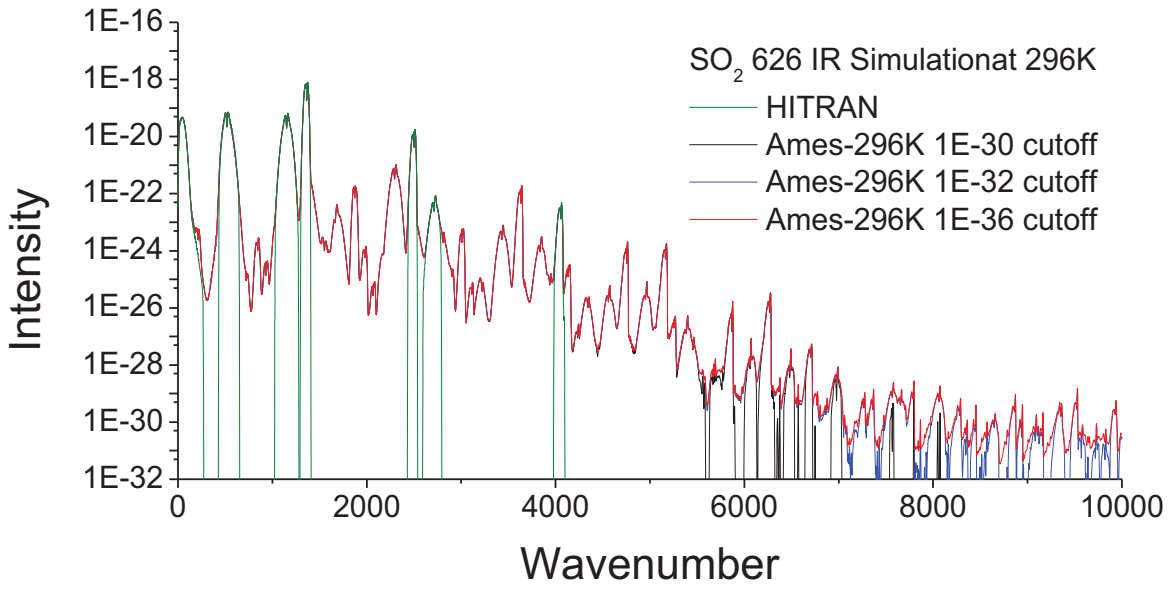

Fig. 5 Ames-300K vs. CDMS comparison: (a) ν_2=0, the pure expt data used in CDMS fit; (b) ν_2=0, the full CDMS; (c) ν_2=1, the pure expt data used in CDMS fit; (d) ν_2=1, the full CDMS.

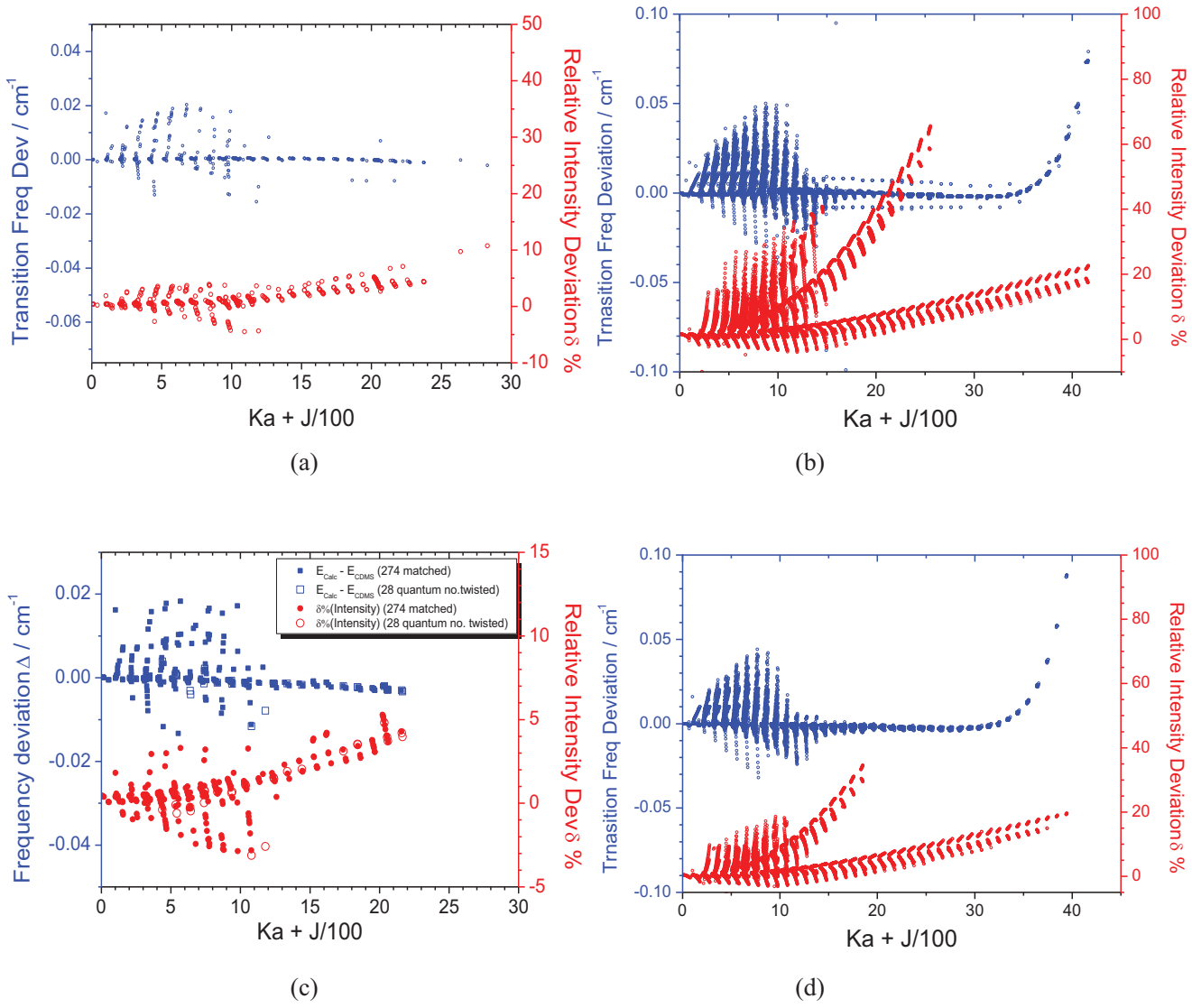

Fig.6 Branched comparison for pure rotational band (ν_2=0) intensity discrepancy, Ames-300K vs. the pure expt data used in CDMS fit.

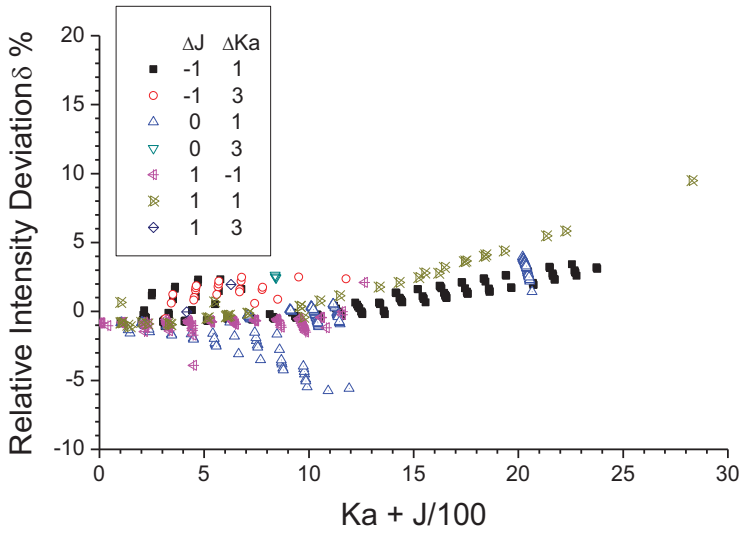

Fig. 7. Ames-296K-based IR simulation (bottom red line) vs. observed $^{32}S^{16}O_2$ $3\nu_1$ *P* branch spectra (top black line, reproduced with permission from J. Mol. Spectrosc. 255, 111 (2009). Copyright 2009 Elsevier Inc.)]).

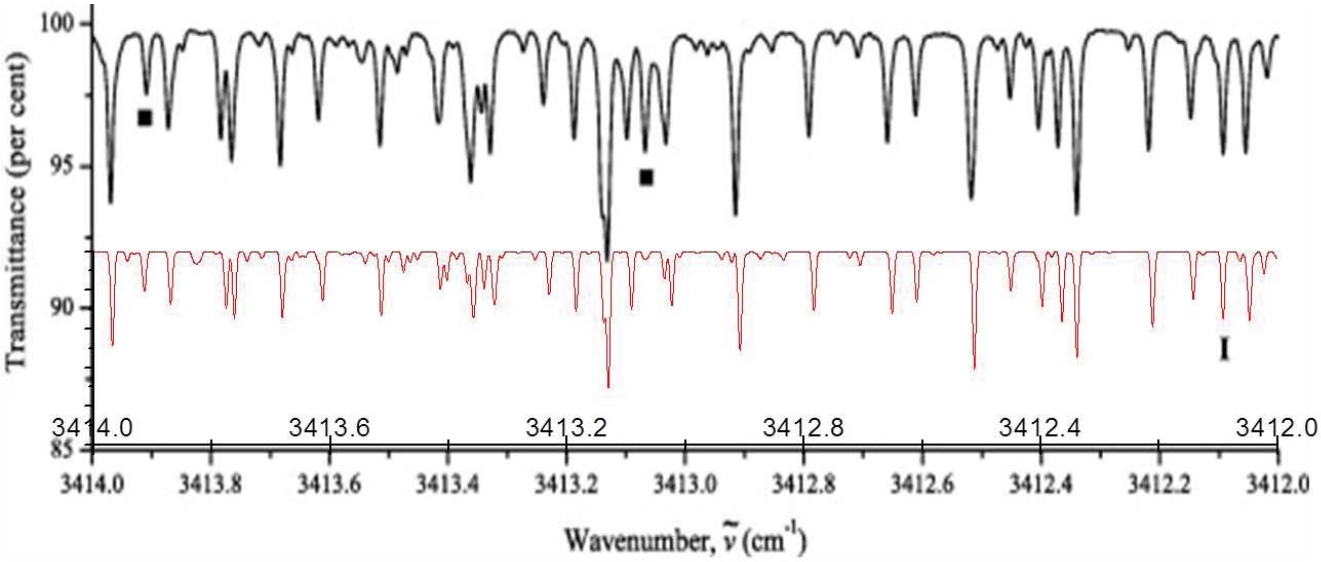

Fig.8. Ames-296K-based IR simulation (bottom red line) vs. observed $^{32}S^{16}O_2$ $\nu_2\nu+_3$ spectra (top black line, reported in Ref.46), including the hot-band $2\nu_2\nu+_3\nu \leftarrow {}_2$ features at right end.

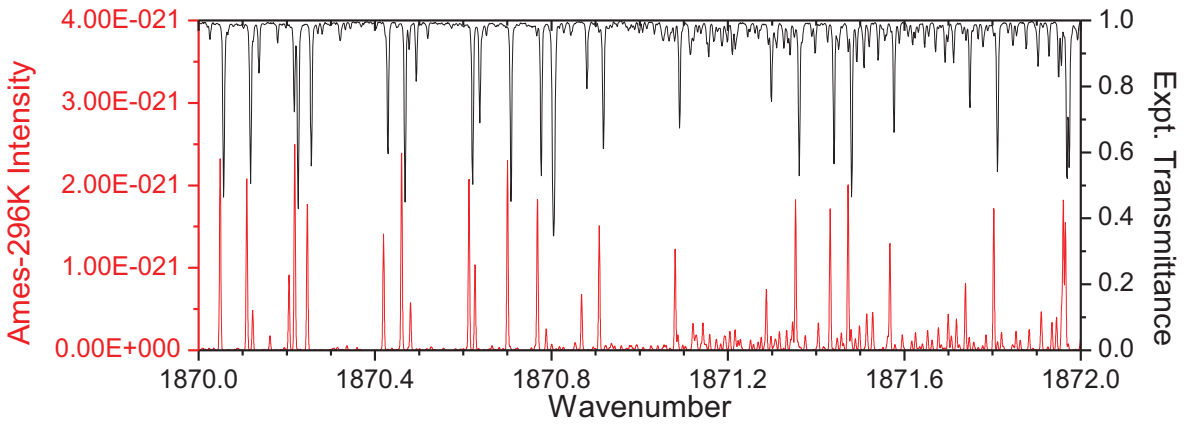

Fig.9 Differences of the GS/ν_1/ν_3/$2\nu_2$ energy levels and transition frequencies between Ames (This work), New Effective Hamiltonian analysis in 2013 (see text for details), and HITRAN data (which is CDMS based): (a) and (b) show the energy level differences, (c) and (d) show the transition wavenumber differences.